AIMS Mathematics, 10(12): 29522–29551.
DOI: 10.3934/math.20251297
Received: 11 October 2025
Revised: 28 November 2025
Accepted: 03 December 2025
Published: 15 December 2025

https://www.aimspress.com/journal/Math

Research article

Hamiltonian analysis and dynamical behavior of bright, dark and other multiple soliton solutions of the Katugampola-fractional reduced spin Hirota-Maxwell-Bloch system

Meshari Alesemi*

Department of Mathematics, College of Science, University of Bisha, P.O. Box 511, Bisha 61922, Saudi Arabia

* **Correspondence:** Email: malesemi@ub.edu.sa.

Abstract: In this research, we investigated the integrable fractional reduced spin Hirota-Maxwell-Bloch system with Katugampola fractional derivatives, a crucial model for analyzing the femtosecond pulses transmitted within an erbium-doped fiber. The modified unified method and the (G'/G)-expansion techniques were employed to acquire analytical soliton solutions comprising bright soliton, mix dark-bright soliton, dark soliton, perturbed dark and bright soliton, multi-soliton, and periodic dark-bright soliton. The fundamental mechanics of the model was revealed by dynamically displaying some of the found solutions using 2D and 3D graphs. The ρ-derivative framework was used to analyze the effect of the space-fractional derivative on the supplied model, offering a more dynamic and applicable way to improve the accuracy of the findings. Additionally, a range of graphical representations were used to show the perturbed system's time series plots and the planar system's phase portraits under the Hamiltonian analysis to emphasize the model's significance and dynamic behavior in erbium-doped fiber. Our findings of this study are expected to have important ramifications for soliton theory, erbium-doped fiber, optical fibers, physical engineering, and nonlinear dynamics. Additionally, the study shows that the $(\frac{G'}{G})$-expansion method and the modified unified approach are simple, robust, and efficient methods that produce many soliton solutions for a range of nonlinear fractional partial differential equations in the mathematical sciences.

Keywords: nonlinear fractional partial differential equations; fractional reduced spin Hirota-Maxwell-Bloch system; Katugampola fractional derivatives; modified unified approach; $(\frac{G'}{G})$-expansion method; hamiltonian analysis; dark and bright soliton solutions
Mathematics Subject Classification: 34G20, 35A20, 35A22, 35R11

1. Introduction

Nonlinear partial differential equations (NPDEs) are being used by scholars and researchers to better comprehend natural phenomena as a result of advances in contemporary science and technology. Many natural contexts, including ocean engineering, plasma physics, hydrodynamics, fluid dynamics, general relativity, optical fibers, quantum mechanics, complex acoustics, geochemistry, finance, and biology, use NPDEs. Because of its special qualities of form retention and constant speed, soliton has a broad variety of applications in many different realms. Soliton wave research and analysis is one area where NPDEs have been used extensively. Scholars have used a number of nonlinear real-world models to anticipate and analyze the properties of soliton waves. Such models comprise dual-mode nonlinear Schrödinger equation in optics [1], Korteweg-de Vries (KdV) equation in water waves [2], Nizhnik-Novikov-Veselov equation in plasma physics [3], Kadomtsev-Petviashvili equation in fluid [4], stochastic modified Gerdjikov-Ivanov equation in optics [5], and so on.

The first international conference on fractional calculus took place in 1974. A traditional integer-order derivative is extended to non-integer orders via a fractional derivative [6]. This progress benefited from the contributions of many notable mathematicians, including Abel, Lagrange, Euler, Riemann, Caputo, Liouville, and many more. Caputo, Riemann-Liouville, Hadamard, Riesz, Caputo-Hadamard, Khalil, Atangana, Oliveira, Sousa, and Katugampola define several kinds of fractional derivatives. The distinctive features of various definitions help explain why fractional calculus is useful in both academic and practical settings. Since, unlike other fractional derivatives, KFD satisfies all Leibniz rules of derivatives [7], it offers a valid tool for modeling complicated systems with non-integer differentiation orders, which is essential for expanding the use of classical calculus to more intricate, practical problems. Fractional derivatives are used in a wide range of disciplines beyond classical calculus, including physics, biology, control systems, engineering, heat and mass transport, electromagnetics, signal processing, and quantum mechanics. One kind of NPDE that includes fractional derivatives in a nonlinear equation is called a Nonlinear Fractional Partial Differential Equation (NFPDE) [8, 9]. By extending the modeling capabilities of conventional NPDEs, NFPDEs may be used for a variety of real-world events that display intricate, memory-dependent, and non-local behaviors [10, 11]. Over the past 10 years, NFPDEs have drawn a lot of attention from the nonlinear sciences community due to the astounding range of possibilities they provide. The closed-form solutions of NFPDEs are now essential for comprehending intricate nonlinear wave processes in most natural sciences. Because of their complexity, NFPDEs are a subject of ongoing research, and new methods for comprehending and resolving them are continually being developed [12].

There are a number of methods for analyzing NFPDEs that provide closed-form wave solutions, such as the extended trial equation technique [13], Riccati modified simple equation method [14], exp-function method [15], the Jacobi elliptic function method [16], the generalized Kudryashov auxiliary method [17], Hirota bilinear method [18], the Kudryashov method [19], the first integral method [20], the sine-cosine method [21], the soliton ansatz technique [22], the tanh-coth method [23], the Riccatti-Bernoulli sub-ODE technique [24], direct algebraic method [25], extended tanh function method [26], the Khater method [27], the (G'/G)-expansion method [28], unified method [29], modified simple equation method [30], and many others have been developed [31–33]. Since its introduction, the (G'/G)-expansion method and unified method have grown to be a widely used mathematical method for solving NPDEs. In the realm of nonlinear mathematical analysis, these methods have shown

tremendous potential. These transformation-based methods that use a wave transformation to convert a NFPDE into an integer order nonlinear ordinary differential equation (NODE). The resulting NODE is further transformed into a nonlinear system of algebraic equations by supposing a closed-form solution. The Maple program is used to evaluate the resultant nonlinear system of algebraic equations in order to find the new plethora of soliton solutions for the NLPDE. Numerous researchers have used these techniques for a number of NFPDEs, finding a range of soliton solutions and wave forms. For instance, the (G'/G)-expansion method was used by Li to study optical solutions of the nonlinear Kodama equation with the M-truncated derivative [34]. Behera solved the Hirota-Ramani equation using the (G'/G)-expansion method and obtained periodic profile, singular periodic profile, M-shape rational profile, singular soliton profile, kink profile, and bright soliton profile in the form of the hyperbolic, rational, and trigonometric solutions [35]. Aydemir applied the generalized unified method to the Biswas-Milovic equation with Kerr, power, parabolic, and dual-power-law nonlinearities to obtain exact solutions [36]. Finally, Raza et al. [37] studied two important temporal fractional nonlinear evolution equations, namely the (1+1)-dimensional Zakharov equation and (2+1)-dimensional Chaffee-Infante equation, by utilizing the unified method along with properties of local M-derivative and obtained optical soliton wave solutions in polynomial and rational forms.

The fractional reduced spin Hirota-Maxwell Bloch system (FRSHMBS), which incorporates Katugampola fractional derivatives (KFDs), is a fractional generalization of the reduced spin Hirota-Maxwell Bloch system (RSHMBS), a significant coupled system in nonlinear optics that accounts for the propagation of femtosecond pulses via optical fibers doped with erbium. The study of femtosecond pulse propagation in optical fibers has gained significant attention due to advancements in ultrafast photonic devices, as femtosecond pulses are crucial for high-speed fiber-optic telecommunication and ultrafast data processing [38–40]. The RSHMBS is particularly important for describing breather waves, rogue waves, and other solitons in erbium-doped media [41–43]. However, the nonlinear Schrödinger equation is being developed to explain the motion of an optical pulse in a single mode fiber at the picosecond regime [44]. It has been discovered that a unique kind of optical pulse, called self induced transparency (SIT), propagates resoundingly across a two-stage absorbing medium without deformation or loss [45]. The propagation of the SIT soliton has been described using the Maxwell-Bloch equations [46]. The propagation of femtosecond pulses via an outer bimetallic doped fiber is described by the coupled system of RSHMBS [47]. This model is expressed as follows [48]:

$$\begin{aligned} &\frac{1}{2}u_{xt} - i\Xi u_t - 2uv = 0, \\ &\delta|u|_t^2 + 2v_x = 0, \end{aligned} \tag{1.1}$$

where $i = \sqrt{-1}$, $u = u(x,t)$ is a complex differential function that regards to the complex envelope of the modulated wave, while the function $v = v(x,t)$ symbolizes the degree of population inversion. Furthermore, Ξ indicates detuning from the erbium ion transitioning frequency, and δ regulates the energy transfer between the medium and field. The first part in Eq (1.1) deals with the evolution of optical fields, whereas the second equation deals with medium dynamics. In Eq (1.1), the term $\frac{1}{2}u_{xt}$ denotes higher-order dispersion effects pertinent to femtosecond pulses, the nonlinear interaction term $-2uv$ explains the energy swap within the optical field and the erbium-doped medium, the term $\delta|u|_t^2$ in the second part of Eq (1.1) indicates that the medium response is influenced by the pulse intensity, the term $2v_x$ depicts the spatial development of the population inversion, and the term $-i\Xi u_t$

indicates frequency detuning from the erbium transition frequency. Furthermore, the soliton solutions of RSHMBS have received very little attention in the literature [48, 49]. Nevertheless, there is no literature analysis of this model in the fractional sense, i.e., FRSHMBS. This claim draws attention to a serious gap in the corpus of research. The literature also indicates that the FRSHMBS's Hamiltonian analysis has not been studied by anyone. Therefore, our aim of this work is to generate a new array of soliton solutions to the integrable FRSHMBS using the unified technique and the (G'/G)-expansion method. The FRSHMBS with KFDs is stated as:

$$\begin{aligned} &\frac{1}{2}{}^{KFD}D_t^{\varrho}({}^{KFD}D_x^{\varrho}u) - i\Xi\,{}^{KFD}D_t^{\varrho}u - 2uv = 0,\\ &\delta\,{}^{KFD}D_t^{\varrho}(|u|^2) + 2\,{}^{KFD}D_x^{\rho}v = 0, \quad 0 < \varrho, \rho \leq 1, \end{aligned} \tag{1.2}$$

where ${}^{KFD}D_x^{\varrho}(\cdot)$ and ${}^{KFD}D_t^{\varrho}(\cdot)$ are KFDs with respect to space and time, respectively. In contrast to the integer order model, the fractional model is more suitable for modeling ultrafast optical events where current wave evolution is influenced by past states. This is because of the fractional derivatives that capture phenomena, such as anomalous dispersion, nonlocal interactions, and memory effects, which integer order derivatives fail to capture. We now define the used KFD [7].

Definition 1.1: Let u: $[0, \infty) \to \mathbb{R}$ and $t > 0$, then the KFD of order ϱ is defined as:

$${}^{KFD}D_t^{\varrho}(u)(t) = \lim_{j\to 0} \frac{u(te^{jt^{-\varrho}}) - u(t)}{j}, \tag{1.3}$$

where $0 < \varrho \leq 1$. If u is ϱ-differentiable in some $(0, n)$, $n > 0$ and $\lim_{t\to 0^+} {}^{KFD}D_t^{\varrho}[u(t)]$ exists, then

$${}^{KFD}D_t^{\varrho}[u(0)] = \lim_{t\to 0^+} {}^{KFD}D_t^{\varrho}[u(t)]. \tag{1.4}$$

The ensuing properties of KFD are essential to the current investigation:

$$\begin{cases} {}^{KFD}D_t^{\varrho}t^m = mt^{m-\varrho},\\ {}^{KFD}D_t^{\varrho}(mu(t) + ns(t)) = m\,{}^{KFD}D_t^{\varrho}u(t) + n\,{}^{KFD}D_t^{\varrho}s(t),\\ {}^{KFD}D_t^{\varrho}(s(t)u(t)) = s(t)\,{}^{KFD}D_t^{\varrho}(u)(t) + u(t)\,{}^{KFD}D_t^{\varrho}(s)(t),\\ {}^{KFD}D_t^{\varrho}(s(u(t))) = s'(u(t))\,{}^{KFD}D_t^{\varrho}(u)(t), \end{cases} \tag{1.5}$$

where $m, n \in R$, while $u(t)$ and $s(t)$ are differentiable functions. The distinctiveness of our built fractional form solutions, which have special characteristics different from the present integer form results, is the main source of inspiration for this study. Given these investigations, we suggest utilizing the unified technique and the (G'/G)-expansion method to investigate the FRSHMBS for the first time to produce soliton solutions, containing bright soliton, mix dark-bright soliton, dark soliton, perturbed dark and bright soliton, multi-soliton, and periodic dark-bright soliton. Using 3D and 2D plots, some of the discovered solutions are dynamically shown, revealing the model's underpinning mechanism. The ρ-derivative framework is used to analyze the effect of the space-fractional derivative on the supplied model, offering a more dynamic and applicable way to improve the accuracy of the findings. In addition, under the Hamiltonian analysis, the planar system's phase portraits and the perturbed system's time series plots are displayed using graphical representations to highlight the model's importance and dynamical behavior in erbium-doped fiber. The results of this investigation are supposed to have

significant implications for nonlinear dynamics, optical fibers, physical engineering, erbium-doped fiber, and soliton theory. Furthermore, we also demonstrate that the modified unified approach and the $(\frac{G'}{G})$-expansion method are effective, resilient, and straightforward techniques that provide a large number of soliton solutions that can be used for a variety of NFPDEs in the mathematical sciences.

The present paper is organized into the following sections: With the application of a wave transformation, the model is reduced to a single integer order governing NODE with some constraint conditions in Section 2; the Hamiltonian analysis of the governing system is conducted in Section 3; In Section 4 we present the structural mechanisms of the used methods. In Section 5, we offer new soliton solutions for FRSHMBS using the suggested approaches. In Section 6, the found soliton solutions are discussed in detail. In the conclusion section, we offer a concise summary of the findings. In the last section, the Appendix, we present a comparison of methods and a list of abbreviations and symbols.

2. Wave transformation and the governing equation

The ensuing wave transformation is initially considered for Eq (1.2):

$$\begin{aligned} &u(x,t) = U(\chi)e^{i\varsigma}, \quad v(x,t) = V(\chi), \\ &\chi = \frac{x^{\rho}}{\rho} + \beta\frac{t^{\varrho}}{\varrho} \quad \text{and} \quad \varsigma = \vartheta\frac{x^{\rho}}{\rho} + \gamma\frac{t^{\varrho}}{\varrho}, \end{aligned} \tag{2.1}$$

where β, ϑ, and γ are wave numbers. This transformation reduces (1.2) to the subsequent set of NODEs:

$$\begin{aligned} &\beta U'' + i\gamma U' + i\vartheta\beta U' - \vartheta\gamma U - 2i\Xi\beta U' + 2\gamma\Xi U - 4UV = 0, \\ &2\delta\beta U U' + 2V' = 0. \end{aligned} \tag{2.2}$$

Splitting the first equation in Eq (2.2) into real and imaginary parts, we acquire:

$$\beta U'' - \gamma(\vartheta - 2\Xi)U - 4UV = 0, \tag{2.3}$$

and

$$(\gamma + \vartheta\beta - 2\Xi\beta)U' = 0. \tag{2.4}$$

Moreover, Eq (2.4) and the second equation in Eq (2.2) (when integrated once w.r.t χ) yield the given constraint conditions:

$$\beta = \frac{\gamma}{2\Xi - \vartheta}, \quad 2\Xi \neq \vartheta, \tag{2.5}$$

and

$$V = -\frac{\gamma\delta}{2(2\Xi - \vartheta)}U^2 + \Lambda, \tag{2.6}$$

respectively, where Λ is a constant of integration. The whole system is reduced to the following single NODE when the constraint conditions in Eqs (2.5) and (2.6) are applied to Eq (2.3):

$$\frac{\gamma U''}{2\,\Xi - \vartheta} - \gamma\,(\vartheta - 2\,\Xi)\,U + \frac{2\delta\,\gamma\,U^3}{(2\,\Xi - \vartheta)} - 4\Lambda U = 0. \tag{2.7}$$

3. Hamiltonian analysis of the system

Various approaches are introduced and used in the literature to analyze the stability and underlying dynamics of nonlinear models [50, 51]. In this section, we provide the governing model's Hamiltonian analysis by presenting equilibrium points, Jacobean matrix, phase portraits, bifurcation analysis, and some time-series plots.

3.1. The Hamiltonian of the dynamical system

With $\Lambda = 0$, the planar dynamical system of Eq (2.7) is obtained as below:

$$\begin{aligned} F(U(\chi), Z(\chi)) &= U'(\chi) = Z(\chi), \\ W(U(\chi), Z(\chi)) &= Z'(\chi) = -(\vartheta - 2\Xi)^2 U(\chi) - 2\delta U^3(\chi), \end{aligned} \tag{3.1}$$

with the Hamiltonian:

$$H(U(\chi), Z(\chi)) = \frac{Z^2(\chi)}{2} + \frac{(\vartheta - 2\Xi)^2}{2} U^2(\chi) + \frac{\delta}{2} U^4(\chi). \tag{3.2}$$

For Eq (3.1), this Hamiltonian gives three equilibrium points: $(0, 0)$, $(U_1, 0)$, and $(U_2, 0)$ along the U-axis where:

$$\begin{aligned} U_1 &= \frac{\vartheta - 2\Xi}{\sqrt{-2\delta}}, \\ U_2 &= -\frac{\vartheta - 2\Xi}{\sqrt{-2\delta}}. \end{aligned} \tag{3.3}$$

Furthermore, using the Jacobian matrix:

$$J = \begin{bmatrix} \frac{\partial F}{\partial U(\chi)} & \frac{\partial F}{\partial Z(\chi)} \\ \frac{\partial W}{\partial U(\chi)} & \frac{\partial W}{\partial Z(\chi)} \end{bmatrix}. \tag{3.4}$$

Equation (3.1) has the ensuing Jacobian:

$$J(U(\chi), Z(\chi)) = \begin{bmatrix} 0 & 1 \\ -(\vartheta - 2\Xi)^2 - 6\delta U(\chi)^2 & 0 \end{bmatrix}, \tag{3.5}$$

with the eigenvalues:

$$EV_i = \pm \sqrt{-(\vartheta - 2\Xi)^2 - 6\delta U(\chi)^2}. \tag{3.6}$$

Any equilibrium point is classified into center or saddle etc. based on the values of eigenvalues of the Jacobian at the equilibrium point, i.e.,

i. At $(U_i, 0), i = 1, 2$, the value of eigenvalues are $EV_i = \pm\sqrt{2}(\vartheta - 2\Xi)$, which implies that the equilibrium points exist and act as saddle points when $\delta < 0$.

ii. At $(0, 0)$, the values of eigenvalues are $EV_i = \pm i(\vartheta - 2\Xi)$, which implies that the equilibrium point always acts as center.

3.1.1. Phase portraits

We first use the phase portraits to demonstrate whether or not the model underpinning the perturbed dynamical system behaves chaotically in order to comprehend this phenomenon. Figures 1 and 2 demonstrate the phase portraits for analysing the existence of periodic/chaotic dynamics in the perturbed nonlinear system under various initial conditions and with correspondingly appropriate parameter values.

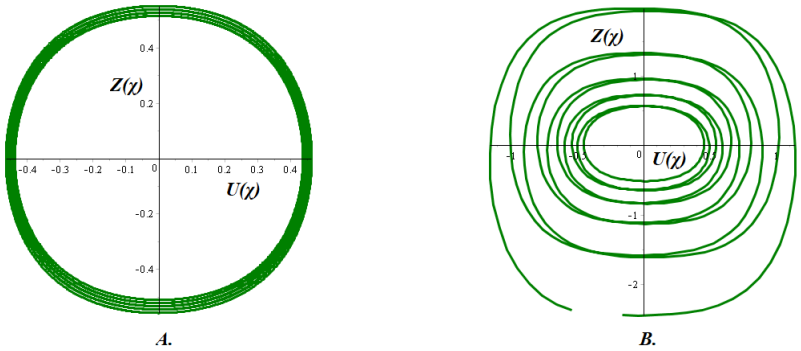

Figure 1. These phase portraits *A*. for stepsize=0.005 and *B*. for stepsize=0.05 of Eq (3.1) are depicted for $\delta = 2, \vartheta = 5, \Xi = 2$. Here, $\delta > 0$ thus, only one equilibrium point $(0, 0)$ exists, which acts as center. The trajectories are closed loops that intersect themselves, revealing periodic or quasi-periodic natures in the model.

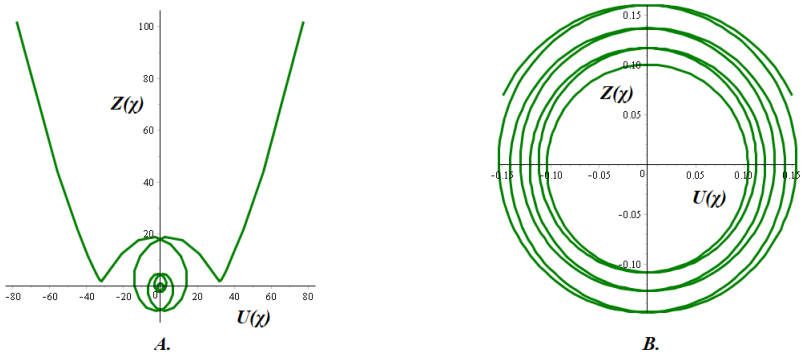

Figure 2. These phase portraits *A*. for stepsize=0.5 and *B*. for stepsize=0.05 of Eq (3.1) are depicted for $\delta = -0.0005, \vartheta = 5, \Xi = 3$. Here, $\delta < 0$, thus, two or three equilibrium points exist, where $(0, 0)$ in *A*. and *B*. acts as the center, while $(U_1, 0) = (31.62277660, 0)$ and $(U_3, 0) = (-31.62277660, 0)$ act as saddle points in *A*. plot. Moreover, in *A*., the motion of trajectory originates as a circle around the center $(0, 0)$, but it deflects symmetrically upward when traverses toward saddle points $(U_1, 0) = (31.62277660, 0)$ and $(U_3, 0) = (-31.62277660, 0)$, which may reflect complex periodic orbits or structural instability. While the trajectory in *B*. is a closed loop that intersects itself, it reveals periodic or quasi-periodic natures in the model. Moreover, the deflection symmetry typically indicates a conservative or symmetric system that is possibly integrable.

Based on the phase portraits, we may arrive at the conclusion that the system is not fully chaotic but may exhibit quasi-periodic or periodic dynamics in part.

3.1.2. Time series plots

In order to perturb the system's periodic motion and obtain useful findings about the chaotic analysis of the governing system of Eq (2.7), we add a perturbation term to the planar dynamical system obtained by transforming Eq (2.7) into a system of first order ordinary differential equations. This system, with the external periodic force, is articulated as:

$$\begin{aligned} F(U(\chi), Z(\chi)) &= U'(\chi) = Z(\chi), \\ Y(U(\chi), Z(\chi)) &= -(\vartheta - 2\Xi)^2 U(\chi) - 2\delta U^3(\chi) + \rho_0 \cos_s(\varrho\chi), \end{aligned} \tag{3.7}$$

where $\cos_s(\varrho\chi)$ is a generalized trigonometric function, while ρ_0 shows the degree and ϱ represents the frequency of the applied external force. We now use the time series approach to demonstrate whether or not the model underpinning the perturbed dynamical system behaves chaotically in order to comprehend this phenomenon. Figures 3 and 4 demonstrate some time-series plots of the governing model for initial conditions and with correspondingly appropriate parameter values.

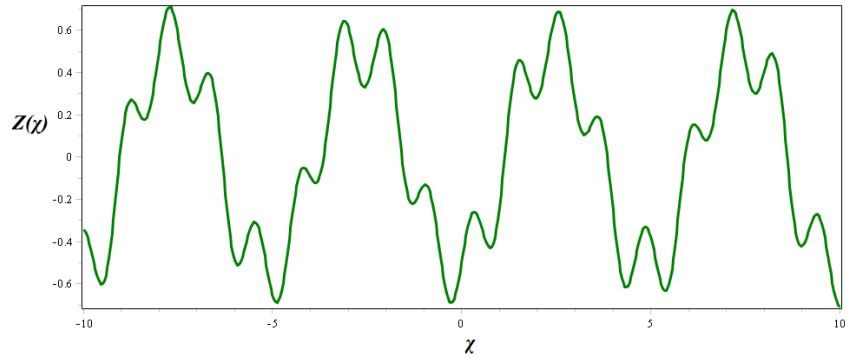

A. The time-series plot of Z(χ)

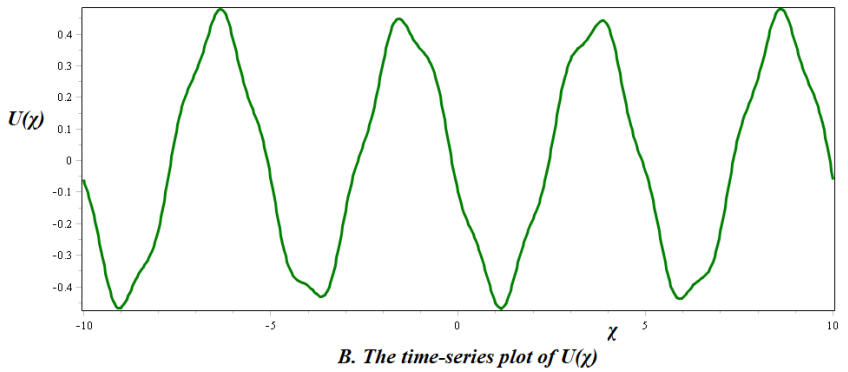

B. The time-series plot of U(χ)

Figure 3. These time-series plots reveal regular and fractal-periodic patterns in the perturbed system represented by Eq (3.7) at $\delta = 2, \vartheta = 5, \Xi = 2, \rho_0 = 1, \varrho = 5$, and $s = 3$, taking the initial conditions $U(0) = -0.1$ and $Z(0) = -0.5$.

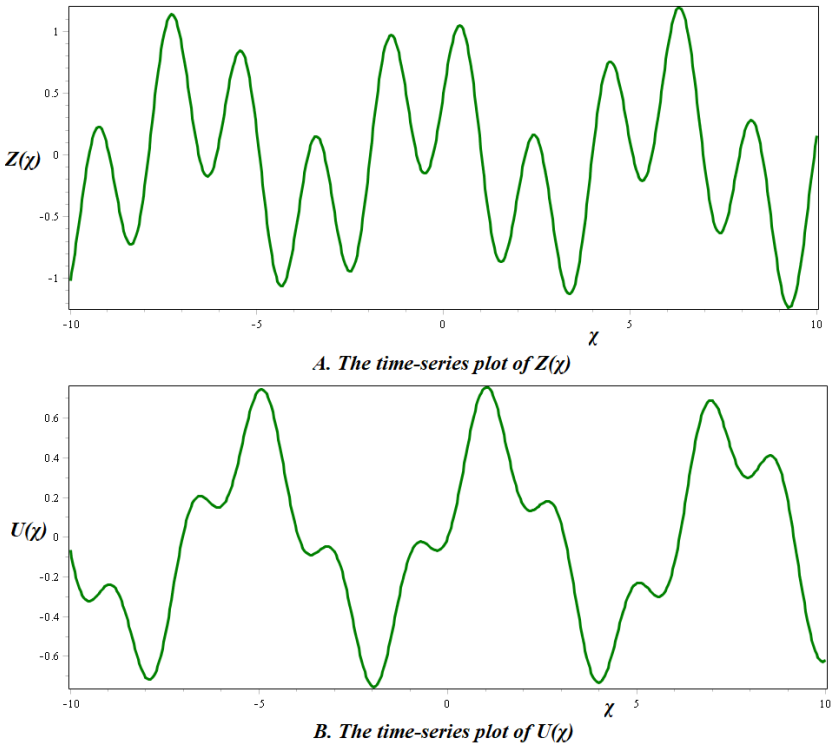

Figure 4. These time-series plots reveal regular and quasi-periodic patterns in the perturbed system represented by Eq (3.7) at $\delta = -0.0005, \vartheta = 5, \Xi = 3, \rho_0 = 2, \varrho = 2$, and $s = 5$ taking the initial conditions $U(0) = 0$ and $Z(0) = 0.5$.

Based on the time-series plots, the system behaves in a periodic and quasi-periodic manner, showing indications of weak or near-fractal chaos in certain areas but not complete chaos.

4. Research methodologies

In this section, we present the working mechanisms of the proposed methods in order to establish soliton solutions for (1.2).

4.1. The operational procedure of $(\frac{G'}{G})$*-expansion method*

In accordance with the methodology in [28], the $(\frac{G'}{G})$-expansion method presumes the following closed-form solution for Eq (2.7):

$$U(\chi) = \sum_{l=-\theta}^{\theta} A_l (\frac{G'(\chi)}{G(\chi)})^l, \tag{4.1}$$

where arbitrary parameters $A_l's (l = -\theta, ..., \theta)$ need to be determined later. The positive integer θ in Eq (4.1) is called the balance number that is determined through the homogenous balance between the nonlinear term and highest derivative in Eq (2.7), while the function $G(\chi)$ represents the solution of the following ordinary differential equation:

$$G''(\chi) + \Phi G'(\chi) + \Omega G(\chi) = 0, \tag{4.2}$$

where Φ, Ω are constants. Furthermore, by the general solution of Eq (4.2), we have:

$$\left(\frac{G'(\chi)}{G(\chi)}\right) = \begin{cases} \frac{1}{2}\,\frac{\sqrt{\Pi}\left(\xi_1 \sinh\left(\frac{1}{2}\,\sqrt{\Pi}\chi\right)+\xi_2 \cosh\left(\frac{1}{2}\,\sqrt{\Pi}\chi\right)\right)}{\xi_1 \cosh\left(\frac{1}{2}\,\sqrt{\Pi}\chi\right)+\xi_2 \sinh\left(\frac{1}{2}\,\sqrt{\Pi}\chi\right)} - \frac{1}{2}\,\Phi, & \Pi > 0, \\ \frac{1}{2}\,\frac{\sqrt{-\Pi}\left(-\xi_1 \sin\left(\frac{1}{2}\,\sqrt{-\Pi}\chi\right)+\xi_2 \cos\left(\frac{1}{2}\,\sqrt{-\Pi}\chi\right)\right)}{\xi_1 \cos\left(\frac{1}{2}\,\sqrt{-\Pi}\chi\right)+\xi_2 \sin\left(\frac{1}{2}\,\sqrt{-\Pi}\chi\right)} - \frac{1}{2}\,\Phi, & \Pi < 0, \\ \frac{\xi_2}{\xi_1+\xi_2\chi} - \frac{1}{2}\,\Phi, & \Pi = 0, \end{cases} \tag{4.3}$$

where $\Pi = \Phi^2 - 4\Omega$ and ξ_1 and ξ_2 in Eq (4.3) are arbitrary constants.

4.2. The operational procedure of the modified unified method

The modified unified method [36] presumes the following closed-form solution for Eq (2.7):

$$U(\chi) = \sum_{l=-\theta}^{\theta} A_l (G(\chi))^l, \tag{4.4}$$

where the function $G(\chi)$ represents the solution of the following ordinary differential equation:

$$G'(\chi) = \Omega + G^2(\chi), \tag{4.5}$$

where Ω is an arbitrary constant. Furthermore, the general solution of Eq (4.5) is presented as:
Solution class 1: When $\Omega < 0$, then:

$$G_1(\chi) = \pm\frac{\sqrt{-\left(g^2+h^2\right)\Omega} - g\,\sqrt{-\Omega}\cosh\left(2\,\sqrt{-\Omega}\,(\chi+\tau)\right)}{g\sinh\left(2\,\sqrt{-\Omega}\,(\chi+\tau)\right)+h}, \tag{4.6}$$

$$G_2(\chi) = \pm\sqrt{-\Omega} + \frac{\mp 2g\,\sqrt{-\Omega}}{g+\cosh\left(2\,\sqrt{-\Omega}\,(\chi+\tau)\right) \mp \ sinh\left(2\,\sqrt{-\Omega}\,(\chi+\tau)\right)}, \tag{4.7}$$

$$G_3(\chi) = \sqrt{-\Omega}\tanh\left(\sqrt{-\Omega}\,(\chi+\tau)\right), \tag{4.8}$$

and

$$G_4(\chi) = \sqrt{-\Omega}\coth\left(\sqrt{-\Omega}\,(\chi+\tau)\right). \tag{4.9}$$

Solution class 2: When $\Omega > 0$, then:

$$G_5(\chi) = \frac{\pm\sqrt{\left(g^2-h^2\right)\Omega} - g\,\sqrt{\Omega}\cos\left(2\,\sqrt{\Omega}\,(\chi+\tau)\right)}{g\sin\left(2\,\sqrt{\Omega}\,(\chi+\tau)\right)+h}, \tag{4.10}$$

$$G_6(\chi) = \pm i\,\sqrt{\Omega} + \frac{\mp 2\,i\alpha\,\sqrt{\Omega}}{g+\cos\left(2\,\sqrt{\Omega}\,(\chi+\tau)\right) \mp \sin\left(2\,\sqrt{\Omega}\,(\chi+\tau)\right)}, \tag{4.11}$$

$$G_7(\chi) = \sqrt{\Omega}\tan\left(\sqrt{\Omega}\,(\chi+\tau)\right), \tag{4.12}$$

and

$$G_8(\chi) = -\sqrt{\Omega}\cot\left(\sqrt{\Omega}\,(\chi+\tau)\right). \tag{4.13}$$

Solution class 3: When $\Omega = 0$, then:

$$G_9(\chi) = \frac{-1}{\chi + \tau}. \tag{4.14}$$

Here, τ, g, and h in Eqs (4.6)–(4.14) are arbitrary real constants.

Key steps: According to the methods outlined above, we then incorporate Eq (4.1) or Eq (4.4) (with the determined value of θ) into Eq (2.7) and collect all terms with the same powers of $\frac{G'(\chi)}{G(\chi)}$ (in $\frac{G'(\chi)}{G(\chi)}$-expansion method) or $G(\chi)$ (in Unified method) to get an expression. By comparing the coefficients of the expression, a nonlinear system of algebraic equations in $A_l's(l = -\theta, ..., \theta)$ and other parameters is obtained. Analytically treating with Maple, this system provides the values of $A_l's(l = -\theta, ..., \theta)$ and other parameters. Finally, by replacing the values of the parameters in Eq (4.1) or Eq (4.4) with the corresponding solutions of the methods, novel plethora of soliton solutions to Eq (1.2) are established. Furthermore, Figure 5 shows the flow chart of the used methodologies and findings.

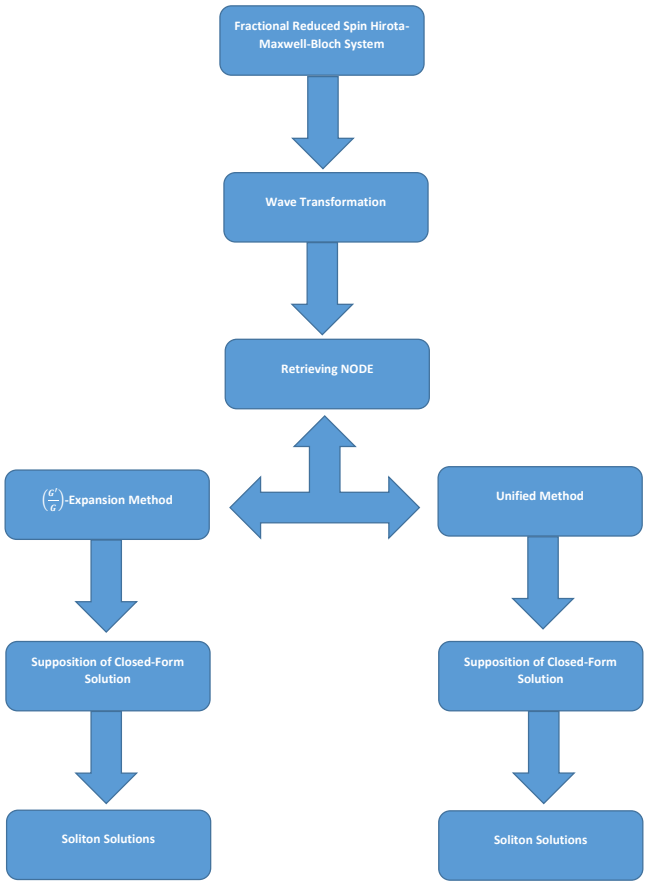

Figure 5. The flow chart of the methodologies.

5. Applications

We now establish novel plethora of soliton solutions for (1.2) utilizing the hired methods.

5.1. The execution of $(\frac{G'(\chi)}{G(\chi)})$*-expansion method*

Establishing the homogenous balance between U^3 and U'', we deduce $\theta = 1$. When $\theta = 1$ is substituted in Eq (4.1), we get the ensuing solution for Eq (2.7):

$$U(\chi) = \sum_{l=-1}^{1} A_l (\frac{G'(\chi)}{G(\chi)})^l. \tag{5.1}$$

An expression in terms of $(\frac{G'(\chi)}{G(\chi)})$ is produced by incorporating Eq (5.1) in Eq (2.7) and combining the alike powered terms of $(\frac{G'(\chi)}{G(\chi)})$. By comparing the coefficients of the expression, a nonlinear system of algebraic equations in $A_l's (l = -1, 0, 1)$ and other parameters is obtained. Analytically treating with Maple, this system provides the subsequent cases types of solutions:

Case. M1.1

$$A_0 = \frac{1}{2}\,\Phi\, A_1, A_1 = A_1, A_{-1} = 0, \vartheta = \vartheta, \delta = -\frac{1}{{A_1}^2}, \gamma = \frac{8\Lambda\ (2\,\Xi - \vartheta)}{8\,\Xi^2 - 8\,\Xi\,\vartheta + 2\,\vartheta^2 - \Pi}, \Xi = \Xi. \tag{5.2}$$

Case. M1.2

$$A_0 = A_0, A_1 = 0, A_{-1} = \frac{2\Omega\, A_0}{\Phi}, \vartheta = \vartheta, \delta = -\frac{\Phi^2}{4{A_0}^2}, \gamma = \frac{8\Lambda\ (2\,\Xi - \vartheta)}{8\,\Xi^2 - 8\,\Xi\,\vartheta + 2\,\vartheta^2 - \Pi}, \Xi = \Xi. \tag{5.3}$$

Assuming case. **M**1.1, we get the following families of solutions for (1.2), where $\chi = \frac{x^\rho}{\rho} + \left(\frac{8\Lambda}{8\,\Xi^2 - 8\,\Xi\,\vartheta + 2\,\vartheta^2 - \Pi}\right)\frac{t^\varrho}{\varrho}$ and $\varsigma = \vartheta\frac{x^\rho}{\rho} + \left(\frac{8\Lambda\,(2\,\Xi - \vartheta)}{8\,\Xi^2 - 8\,\Xi\,\vartheta + 2\,\vartheta^2 - \Pi}\right)\frac{t^\varrho}{\varrho}$:

Solution class. M1.1.1: Hyperbolic function solutions (when $\Pi > 0$):
(i) When $\xi_1 \neq 0, \xi_2 \neq 0$:

$$\begin{aligned} u_{\mathrm{M1},1,1}(x,t) =& \mathrm{e}^{i\varsigma}\Big(\frac{A_1}{2}\,\frac{\sqrt{\Pi}\left(\xi_1 \sinh\left(\frac{1}{2}\,\sqrt{\Pi}\chi\right) + \xi_2 \cosh\left(\frac{1}{2}\,\sqrt{\Pi}\chi\right)\right)}{\xi_1 \cosh\left(\frac{1}{2}\,\sqrt{\Pi}\chi\right) + \xi_2 \sinh\left(\frac{1}{2}\,\sqrt{\Pi}\chi\right)}\Big), \\ v_{\mathrm{M1},1,1}(x,t) =& \frac{\Lambda}{(8\,\Xi^2 - 8\,\Xi\,\vartheta + 2\,\vartheta^2 - \Pi)}\Big(\frac{\sqrt{\Pi}\left(\xi_1 \sinh\left(\frac{1}{2}\,\sqrt{\Pi}\chi\right) + \xi_2 \cosh\left(\frac{1}{2}\,\sqrt{\Pi}\chi\right)\right)}{\xi_1 \cosh\left(\frac{1}{2}\,\sqrt{\Pi}\chi\right) + \xi_2 \sinh\left(\frac{1}{2}\,\sqrt{\Pi}\chi\right)}\Big)^2 + \Lambda. \end{aligned} \tag{5.4}$$

(ii) When $\xi_1 = 0, \xi_2 \neq 0$:

$$\begin{aligned} u_{\mathrm{M1},1,2}(x,t) =& \mathrm{e}^{i\varsigma}\Big(\frac{A_1}{2}\,\sqrt{\Pi}\coth\left(\frac{1}{2}\,\sqrt{\Pi}\chi\right)\Big), \\ v_{\mathrm{M1},1,2}(x,t) =& \frac{\Lambda}{(8\,\Xi^2 - 8\,\Xi\,\vartheta + 2\,\vartheta^2 - \Pi)}\Big(\sqrt{\Pi}\coth\left(\frac{1}{2}\,\sqrt{\Pi}\chi\right)\Big)^2 + \Lambda. \end{aligned} \tag{5.5}$$

(iii) When $\xi_1 \neq 0, \xi_2 = 0$:

$$\begin{aligned} u_{\mathrm{M1,1,3}}(x,t) =& \mathrm{e}^{i\varsigma}\Big(\frac{A_1}{2}\ \sqrt{\Pi}\tanh\Big(\frac{1}{2}\ \sqrt{\Pi}\chi\Big)\Big), \\ v_{\mathrm{M1,1,3}}(x,t) =& \frac{\Lambda}{(8\,\Xi^2 - 8\,\Xi\,\vartheta + 2\,\vartheta^2 - \Pi)}\Big(\sqrt{\Pi}\tanh\Big(\frac{1}{2}\ \sqrt{\Pi}\chi\Big)\Big)^2 + \Lambda. \end{aligned} \tag{5.6}$$

Solution class. M1.1.2: Trigonometric function solutions (when $\Pi < 0$):
(i) When $\xi_1 \neq 0, \xi_2 \neq 0$:

$$\begin{aligned} u_{\mathrm{M1,1,4}}(x,t) =& \mathrm{e}^{i\varsigma}\Big(\frac{A_1}{2}\ \frac{\sqrt{-\Pi}\left(-\xi_1\sin\left(\frac{1}{2}\ \sqrt{-\Pi}\chi\right) + \xi_2\cos\left(\frac{1}{2}\ \sqrt{-\Pi}\chi\right)\right)}{\xi_1\cos\left(\frac{1}{2}\ \sqrt{-\Pi}\chi\right) + \xi_2\sin\left(\frac{1}{2}\ \sqrt{-\Pi}\chi\right)}\Big), \\ v_{\mathrm{M1,1,4}}(x,t) =& \frac{\Lambda}{(8\,\Xi^2 - 8\,\Xi\,\vartheta + 2\,\vartheta^2 - \Pi)}\Big(\frac{\sqrt{-\Pi}\left(-\xi_1\sin\left(\frac{1}{2}\ \sqrt{-\Pi}\chi\right) + \xi_2\cos\left(\frac{1}{2}\ \sqrt{-\Pi}\chi\right)\right)}{\xi_1\cos\left(\frac{1}{2}\ \sqrt{-\Pi}\chi\right) + \xi_2\sin\left(\frac{1}{2}\ \sqrt{-\Pi}\chi\right)}\Big)^2 + \Lambda. \end{aligned} \tag{5.7}$$

(ii) When $\xi_1 = 0, \xi_2 \neq 0$:

$$\begin{aligned} u_{\mathrm{M1,1,5}}(x,t) =& \mathrm{e}^{i\varsigma}\Big(\frac{A_1}{2}\ \sqrt{-\Pi}\cot\Big(\frac{1}{2}\ \sqrt{-\Pi}\chi\Big)\Big), \\ v_{\mathrm{M1,1,5}}(x,t) =& \frac{\Lambda}{(8\,\Xi^2 - 8\,\Xi\,\vartheta + 2\,\vartheta^2 - \Pi)}\Big(\sqrt{-\Pi}\cot\Big(\frac{1}{2}\ \sqrt{-\Pi}\chi\Big)\Big)^2 + \Lambda. \end{aligned} \tag{5.8}$$

(iii) When $\xi_1 \neq 0, \xi_2 = 0$:

$$\begin{aligned} u_{\mathrm{M1,1,6}}(x,t) =& \mathrm{e}^{i\varsigma}\Big(-\frac{A_1}{2}\ \sqrt{-\Pi}\tan\Big(\frac{1}{2}\ \sqrt{-\Pi}\chi\Big)\Big), \\ v_{\mathrm{M1,1,6}}(x,t) =& \frac{\Lambda}{(8\,\Xi^2 - 8\,\Xi\,\vartheta + 2\,\vartheta^2 - \Pi)}\Big(\sqrt{-\Pi}\tan\Big(\frac{1}{2}\ \sqrt{-\Pi}\chi\Big)\Big)^2 + \Lambda. \end{aligned} \tag{5.9}$$

Solution class. M1.1.3: Rational function solutions (when $\Pi = 0$):
(i) When $\xi_1 \neq 0, \xi_2 \neq 0$:

$$\begin{aligned} u_{\mathrm{M1,1,7}}(x,t) =& \mathrm{e}^{i\varsigma}\Big(\frac{1}{2}\,\Phi\,A_1 + \frac{A_1\xi_2}{\chi\,\xi_2 + \xi_1}\Big), \\ v_{\mathrm{M1,1,7}}(x,t) =& \frac{4\Lambda}{(8\,\Xi^2 - 8\,\Xi\,\vartheta + 2\,\vartheta^2)}\Big(\frac{1}{2}\,\Phi\ + \frac{\xi_2}{\chi\,\xi_2 + \xi_1}\Big)^2 + \Lambda. \end{aligned} \tag{5.10}$$

(ii) When $\xi_1 = 0, \xi_2 \neq 0$:

$$\begin{aligned} u_{\mathrm{M1,1,8}}(x,t) =& \mathrm{e}^{i\varsigma}\Big(\frac{A_1}{\chi}\Big), \\ v_{\mathrm{M1,1,8}}(x,t) =& \frac{4\Lambda}{\chi^2\,(8\,\Xi^2 - 8\,\Xi\,\vartheta + 2\,\vartheta^2)} + \Lambda. \end{aligned} \tag{5.11}$$

Assuming case. **M**1.2, we get the following families of solutions, where $\chi = \frac{x^{\rho}}{\rho} + \left(\frac{8\Lambda}{8\,\Xi^2-8\,\Xi\,\vartheta+2\,\vartheta^2-\Pi}\right)\frac{t^{\varrho}}{\varrho}$ and $\varsigma = \vartheta\frac{x^{\rho}}{\rho} + \left(\frac{8\Lambda\,(2\,\Xi-\vartheta)}{8\,\Xi^2-8\,\Xi\,\vartheta+2\,\vartheta^2-\Pi}\right)\frac{t^{\varrho}}{\varrho}$:

Solution class. M1.2.1: Hyperbolic function solutions (when $\Pi > 0$):
(i) When $\xi_1 \neq 0, \xi_2 \neq 0$:

$$\begin{aligned} u_{\mathrm{M1,2,1}}(x,t) =& e^{i\varsigma}\left(\frac{2\,\Omega\,A_0}{\Phi\left(\frac{1}{2}\,\frac{\sqrt{\Pi}\left(\xi_1\sinh\left(\frac{1}{2}\,\sqrt{\Pi}\chi\right)+\xi_2\cosh\left(\frac{1}{2}\,\sqrt{\Pi}\chi\right)\right)}{\xi_1\cosh\left(\frac{1}{2}\,\sqrt{\Pi}\chi\right)+\xi_2\sinh\left(\frac{1}{2}\,\sqrt{\Pi}\chi\right)}-\frac{1}{2}\,\Phi\right)}+A_0\right),\\ v_{\mathrm{M1,2,1}}(x,t) =& \frac{\Phi^2\Lambda}{{A_0}^2\,(8\,\Xi^2-8\,\Xi\,\vartheta+2\,\vartheta^2-\Pi)}\left(\frac{2\,\Omega\,A_0}{\Phi\left(\frac{1}{2}\,\frac{\sqrt{\Pi}\left(\xi_1\sinh\left(\frac{1}{2}\,\sqrt{\Pi}\chi\right)+\xi_2\cosh\left(\frac{1}{2}\,\sqrt{\Pi}\chi\right)\right)}{\xi_1\cosh\left(\frac{1}{2}\,\sqrt{\Pi}\chi\right)+\xi_2\sinh\left(\frac{1}{2}\,\sqrt{\Pi}\chi\right)}-\frac{1}{2}\,\Phi\right)}+A_0\right)^2+\Lambda. \end{aligned} \tag{5.12}$$

(ii) When $\xi_1 = 0, \xi_2 \neq 0$:

$$\begin{aligned} u_{\mathrm{M1,2,2}}(x,t) =& e^{i\varsigma}\left(2\,\frac{\Omega\,A_0}{\Phi\left(\frac{1}{2}\,\sqrt{\Pi}\coth\left(\frac{1}{2}\,\sqrt{\Pi}\chi\right)-\frac{1}{2}\,\Phi\right)}+A_0\right),\\ v_{\mathrm{M1,2,2}}(x,t) =& \frac{\Phi^2\Lambda}{{A_0}^2\,(8\,\Xi^2-8\,\Xi\,\vartheta+2\,\vartheta^2-\Pi)}\left(2\,\frac{\Omega\,A_0}{\Phi\left(\frac{1}{2}\,\sqrt{\Pi}\coth\left(\frac{1}{2}\,\sqrt{\Pi}\chi\right)-\frac{1}{2}\,\Phi\right)}+A_0\right)^2+\Lambda. \end{aligned} \tag{5.13}$$

(iii) When $\xi_1 \neq 0, \xi_2 = 0$:

$$\begin{aligned} u_{\mathrm{M1,2,3}}(x,t) =& e^{i\varsigma}\left(2\,\frac{\Omega\,A_0}{\Phi\left(\frac{1}{2}\,\sqrt{\Pi}\tanh\left(\frac{1}{2}\,\sqrt{\Pi}\chi\right)-\frac{1}{2}\,\Phi\right)}+A_0\right),\\ v_{\mathrm{M1,2,3}}(x,t) =& \frac{\Phi^2\Lambda}{{A_0}^2\,(8\,\Xi^2-8\,\Xi\,\vartheta+2\,\vartheta^2-\Pi)}\left(2\,\frac{\Omega\,A_0}{\Phi\left(\frac{1}{2}\,\sqrt{\Pi}\tanh\left(\frac{1}{2}\,\sqrt{\Pi}\chi\right)-\frac{1}{2}\,\Phi\right)}+A_0\right)^2+\Lambda. \end{aligned} \tag{5.14}$$

Solution class. M1.2.2: Trigonometric function solutions (when $\Pi < 0$):
(i) When $\xi_1 \neq 0, \xi_2 \neq 0$:

$$\begin{aligned} u_{\mathrm{M1,2,4}}(x,t) =& e^{i\varsigma}\left(\frac{2\,\Omega\,A_0}{\Phi\left(\frac{1}{2}\,\frac{\sqrt{-\Pi}\left(-\xi_1\sin\left(\frac{1}{2}\,\sqrt{-\Pi}\chi\right)+\xi_2\cos\left(\frac{1}{2}\,\sqrt{-\Pi}\chi\right)\right)}{\xi_1\cos\left(\frac{1}{2}\,\sqrt{-\Pi}\chi\right)+\xi_2\sin\left(\frac{1}{2}\,\sqrt{-\Pi}\chi\right)}-\frac{1}{2}\,\Phi\right)}+A_0\right),\\ v_{\mathrm{M1,2,4}}(x,t) =& \frac{\Phi^2\Lambda}{{A_0}^2\,(8\,\Xi^2-8\,\Xi\,\vartheta+2\,\vartheta^2-\Pi)}\left(\frac{2\,\Omega\,A_0}{\Phi\left(\frac{1}{2}\,\frac{\sqrt{-\Pi}\left(-\xi_1\sin\left(\frac{1}{2}\,\sqrt{-\Pi}\chi\right)+\xi_2\cos\left(\frac{1}{2}\,\sqrt{-\Pi}\chi\right)\right)}{\xi_1\cos\left(\frac{1}{2}\,\sqrt{-\Pi}\chi\right)+\xi_2\sin\left(\frac{1}{2}\,\sqrt{-\Pi}\chi\right)}-\frac{1}{2}\,\Phi\right)}+A_0\right)^2+\Lambda. \end{aligned} \tag{5.15}$$

(ii) When $\xi_1 = 0, \xi_2 \neq 0$:

$$\begin{aligned} u_{\mathrm{M1,2,5}}(x,t) =& e^{i\varsigma}\left(2\,\frac{\Omega\,A_0}{\Phi\left(\frac{1}{2}\,\sqrt{-\Pi}\cot\left(\frac{1}{2}\,\sqrt{-\Pi}\chi\right)-\frac{1}{2}\,\Phi\right)}+A_0\right),\\ v_{\mathrm{M1,2,5}}(x,t) =& \frac{\Phi^2\Lambda}{{A_0}^2\,(8\,\Xi^2-8\,\Xi\,\vartheta+2\,\vartheta^2-\Pi)}\left(2\,\frac{\Omega\,A_0}{\Phi\left(\frac{1}{2}\,\sqrt{-\Pi}\cot\left(\frac{1}{2}\,\sqrt{-\Pi}\chi\right)-\frac{1}{2}\,\Phi\right)}+A_0\right)^2+\Lambda. \end{aligned} \tag{5.16}$$

(iii) When $\xi_1 \neq 0, \xi_2 = 0$:

$$\begin{aligned} u_{\mathrm{M1,2,6}}(x,t) =& \mathrm{e}^{i\varsigma}\Big(2\,\frac{\Omega A_0}{\Phi\left(-\frac{1}{2}\,\sqrt{-\Pi}\tan\left(\frac{1}{2}\,\sqrt{-\Pi}\chi\right)-\frac{1}{2}\,\Phi\right)}+A_0\Big), \\ v_{\mathrm{M1,2,6}}(x,t) =& \frac{\Phi^2\Lambda}{{A_0}^2\left(8\,\Xi^2-8\,\Xi\,\vartheta+2\,\vartheta^2-\Pi\right)}\Big(2\,\frac{\Omega A_0}{\Phi\left(-\frac{1}{2}\,\sqrt{-\Pi}\tan\left(\frac{1}{2}\,\sqrt{-\Pi}\chi\right)-\frac{1}{2}\,\Phi\right)}+A_0\Big)^2+\Lambda. \end{aligned} \tag{5.17}$$

Solution class. M1.2.3: Rational function solutions (when $\Pi = 0$):
(i) When $\xi_1 \neq 0, \xi_2 \neq 0$:

$$\begin{aligned} u_{\mathrm{M1,2,7}}(x,t) =& \mathrm{e}^{i\varsigma}\Big(\frac{2\Omega A_0\left(\chi\,\xi_2+\xi_1\right)}{\Phi\,\xi_2}+A_0\Big), \\ v_{\mathrm{M1,2,7}}(x,t) =& \frac{\Phi^2\Lambda}{{A_0}^2\left(8\,\Xi^2-8\,\Xi\,\vartheta+2\,\vartheta^2\right)}\Big(\frac{2\Omega A_0\left(\chi\,\xi_2+\xi_1\right)}{\Phi\,\xi_2}+A_0\Big)^2+\Lambda. \end{aligned} \tag{5.18}$$

(ii) When $\xi_1 = 0, \xi_2 \neq 0$:

$$\begin{aligned} u_{\mathrm{M1,2,8}}(x,t) =& \mathrm{e}^{i\varsigma}\Big(\frac{2\Omega A_0}{\Phi\left(\chi^{-1}-\frac{1}{2}\,\Phi\right)}+A_0\Big), \\ v_{\mathrm{M1,2,8}}(x,t) =& \frac{\Phi^2\Lambda}{{A_0}^2\left(8\,\Xi^2-8\,\Xi\,\vartheta+2\,\vartheta^2\right)}\Big(\frac{2\Omega A_0}{\Phi\left(\chi^{-1}-\frac{1}{2}\,\Phi\right)}+A_0\Big)^2+\Lambda. \end{aligned} \tag{5.19}$$

(iii) When $\xi_1 \neq 0, \xi_2 = 0$:

$$\begin{aligned} u_{\mathrm{M1,2,9}}(x,t) =& \mathrm{e}^{i\varsigma}\Big(\frac{-4\Omega A_0}{\Phi^2}+A_0\Big), \\ v_{\mathrm{M1,2,9}}(x,t) =& \frac{\Phi^2\Lambda}{{A_0}^2\left(8\,\Xi^2-8\,\Xi\,\vartheta+2\,\vartheta^2\right)}\Big(\frac{-4\Omega A_0}{\Phi^2}+A_0\Big)^2+\Lambda. \end{aligned} \tag{5.20}$$

5.2. The execution of the modified unified method

When $\theta = 1$ is substituted in Eq (4.4), we get the ensuing solution for Eq (2.7):

$$U(\chi) = \sum_{l=-1}^{1} A_l (G(\chi))^l. \tag{5.21}$$

An expression in terms of $G(\chi)$ is produced by incorporating Eq (5.21) in Eq (2.7) and combining the alike powered terms of $G(\chi)$. By comparing the coefficients of the expression, a nonlinear system of algebraic equations in $A_l's (l = -1, 0, 1)$ and other parameters is obtained. Analytically treating with Maple, this system provides the subsequent cases types of solutions:

Case. M2.2.1

$$A_0 = 0, A_1 = 0, A_{-1} = \sqrt{-\frac{1}{\delta}}\Omega, \vartheta = \frac{2\,\gamma\,\Xi - 2\,\Lambda + \sqrt{-2\,\Omega\,\gamma^2 + 4\,\Lambda^2}}{\gamma}, \delta = \delta(\neq 0), \gamma = \gamma, \Xi = \Xi. \tag{5.22}$$

Case. M2.2.2

$$A_0 = 0, A_1 = -\sqrt{-\frac{1}{\delta}}, A_{-1} = 0, \vartheta = \frac{2\,\gamma\,\Xi - 2\,\Lambda - \sqrt{-2\,\Omega\,\gamma^2 + 4\,\Lambda^2}}{\gamma}, \delta = \delta(\neq 0), \gamma = \gamma, \Xi = \Xi. \quad (5.23)$$

Assuming case. **M**2.1, we get the following families of solutions, where $\chi = \frac{x^\rho}{\rho} + \left(\frac{\gamma^2}{2\,\Lambda - \sqrt{-2\,\Omega\,\gamma^2+4\,\Lambda^2}}\right)\frac{t^\varrho}{\varrho}$ and $\varsigma = \left(\frac{2\,\gamma\,\Xi - 2\,\Lambda + \sqrt{-2\,\Omega\,\gamma^2+4\,\Lambda^2}}{\gamma}\right)\frac{x^\rho}{\rho} + \gamma\frac{t^\varrho}{\varrho}$:

Solution class. M2.1.1 Hyperbolic function solutions (when $\Omega < 0$):

$$\begin{aligned}
u_{\mathrm{M2},1,1}(x,t) =& e^{i\varsigma}\left(\frac{\sqrt{-\frac{1}{\delta}}\Omega\left(g\sinh\left(2\sqrt{-\Omega}\,(\chi+\tau)\right)+h\right)}{\left(\sqrt{-(g^2+h^2)\,\Omega} - g\sqrt{-\Omega}\cosh\left(2\sqrt{-\Omega}\,(\chi+\tau)\right)\right)}\right),\\
v_{\mathrm{M2},1,1}(x,t) =& -\frac{1}{2}\,\frac{\delta\,\gamma^2}{2\,\Lambda - \sqrt{-2\,\Omega\,\gamma^2+4\,\Lambda^2}}\left(\frac{\sqrt{-\frac{1}{\delta}}\Omega\left(g\sinh\left(2\sqrt{-\Omega}\,(\chi+\tau)\right)+h\right)}{\left(\sqrt{-(g^2+h^2)\,\Omega} - g\sqrt{-\Omega}\cosh\left(2\sqrt{-\Omega}\,(\chi+\tau)\right)\right)}\right)^2 + \Lambda,
\end{aligned} \quad (5.24)$$

$$\begin{aligned}
u_{\mathrm{M2},1,2}(x,t) =& e^{i\varsigma}\left(\frac{\sqrt{-\frac{1}{\delta}}\Omega}{\left(\sqrt{-\Omega} - 2\,\frac{g\sqrt{-\Omega}}{g+\cosh\left(2\sqrt{-\Omega}(\chi+\tau)\right)-\sinh\left(2\sqrt{-\Omega}(\chi+\tau)\right)}\right)}\right),\\
v_{\mathrm{M2},1,2}(x,t) =& -\frac{1}{2}\,\frac{\delta\,\gamma^2}{2\,\Lambda - \sqrt{-2\,\Omega\,\gamma^2+4\,\Lambda^2}}\left(\frac{\sqrt{-\frac{1}{\delta}}\Omega}{\left(\sqrt{-\Omega} - 2\,\frac{g\sqrt{-\Omega}}{g+\cosh\left(2\sqrt{-\Omega}(\chi+\tau)\right)-\sinh\left(2\sqrt{-\Omega}(\chi+\tau)\right)}\right)}\right)^2 + \Lambda,
\end{aligned} \quad (5.25)$$

$$\begin{aligned}
u_{\mathrm{M2},1,3}(x,t) =& e^{i\varsigma}\left(\sqrt{\frac{\Omega}{\delta}}\coth\left(\sqrt{-\Omega}\,(\chi+\tau)\right)\right),\\
v_{\mathrm{M2},1,3}(x,t) =& -\frac{1}{2}\,\frac{\delta\,\gamma^2}{2\,\Lambda - \sqrt{-2\,\Omega\,\gamma^2+4\,\Lambda^2}}\left(\sqrt{\frac{\Omega}{\delta}}\coth\left(\sqrt{-\Omega}\,(\chi+\tau)\right)\right)^2 + \Lambda,
\end{aligned} \quad (5.26)$$

and

$$\begin{aligned}
u_{\mathrm{M2},1,4}(x,t) =& e^{i\varsigma}\left(\sqrt{\frac{\Omega}{\delta}}\tanh\left(\sqrt{-\Omega}\,(\chi+\tau)\right)\right),\\
v_{\mathrm{M2},1,4}(x,t) =& -\frac{1}{2}\,\frac{\delta\,\gamma^2}{2\,\Lambda - \sqrt{-2\,\Omega\,\gamma^2+4\,\Lambda^2}}\left(\sqrt{\frac{\Omega}{\delta}}\tanh\left(\sqrt{-\Omega}\,(\chi+\tau)\right)\right)^2 + \Lambda.
\end{aligned} \quad (5.27)$$

Solution class. M2.1.2 Trigonometric function solutions (when $\Omega > 0$):

$$\begin{aligned}
u_{\mathrm{M2},1,5}(x,t) =& e^{i\varsigma}\left(\frac{\sqrt{-\frac{1}{\delta}}\Omega\left(g\sin\left(2\sqrt{\Omega}\,(\chi+\tau)\right)+h\right)}{\left(\sqrt{(g^2-h^2)\,\Omega} - g\sqrt{\Omega}\cos\left(2\sqrt{\Omega}\,(\chi+\tau)\right)\right)}\right),\\
v_{\mathrm{M2},1,5}(x,t) =& -\frac{1}{2}\,\frac{\delta\,\gamma^2}{2\,\Lambda - \sqrt{-2\,\Omega\,\gamma^2+4\,\Lambda^2}}\left(\frac{\sqrt{-\frac{1}{\delta}}\Omega\left(g\sin\left(2\sqrt{\Omega}\,(\chi+\tau)\right)+h\right)}{\left(\sqrt{(g^2-h^2)\,\Omega} - g\sqrt{\Omega}\cos\left(2\sqrt{\Omega}\,(\chi+\tau)\right)\right)}\right)^2 + \Lambda,
\end{aligned} \quad (5.28)$$

$$
\begin{aligned}
u_{\mathrm{M2,1,6}}(x,t) =& \mathrm{e}^{i\varsigma}\left(\frac{\sqrt{-\frac{1}{\delta}}\Omega}{\left(i\sqrt{\Omega}-\frac{2ig\sqrt{\Omega}}{g+\cos\left(2\sqrt{\Omega}(\chi+\tau)\right)-\sin\left(2\sqrt{\Omega}(\chi+\tau)\right)}\right)}\right),\\
v_{\mathrm{M2,1,6}}(x,t) =& -\frac{1}{2}\,\frac{\delta\gamma^2}{2\Lambda-\sqrt{-2\Omega\gamma^2+4\Lambda^2}}\left(\frac{\sqrt{-\frac{1}{\delta}}\Omega}{\left(i\sqrt{\Omega}-\frac{2ig\sqrt{\Omega}}{g+\cos\left(2\sqrt{\Omega}(\chi+\tau)\right)-\sin\left(2\sqrt{\Omega}(\chi+\tau)\right)}\right)}\right)^2+\Lambda,
\end{aligned}
\tag{5.29}
$$

$$
\begin{aligned}
u_{\mathrm{M2,1,7}}(x,t) =& \mathrm{e}^{i\varsigma}\left(\sqrt{-\frac{\Omega}{\delta}}\cot\left(\sqrt{\Omega}(\chi+\tau)\right)\right),\\
v_{\mathrm{M2,1,7}}(x,t) =& -\frac{1}{2}\,\frac{\delta\gamma^2}{2\Lambda-\sqrt{-2\Omega\gamma^2+4\Lambda^2}}\left(\sqrt{-\frac{\Omega}{\delta}}\cot\left(\sqrt{\Omega}(\chi+\tau)\right)\right)^2+\Lambda,
\end{aligned}
\tag{5.30}
$$

and

$$
\begin{aligned}
u_{\mathrm{M2,1,8}}(x,t) =& \mathrm{e}^{i\varsigma}\left(-\sqrt{-\frac{\Omega}{\delta}}\tan\left(\sqrt{\Omega}(\chi+\tau)\right)\right),\\
v_{\mathrm{M2,1,8}}(x,t) =& -\frac{1}{2}\,\frac{\delta\gamma^2}{2\Lambda-\sqrt{-2\Omega\gamma^2+4\Lambda^2}}\left(-\sqrt{-\frac{\Omega}{\delta}}\tan\left(\sqrt{\Omega}(\chi+\tau)\right)\right)^2+\Lambda.
\end{aligned}
\tag{5.31}
$$

Now assuming case. **M**2.2, we get the following families of solutions, where $\chi = \frac{x^\rho}{\rho} + \left(\frac{\gamma^2}{2\Lambda+\sqrt{-2\Omega\gamma^2+4\Lambda^2}}\right)\frac{t^\varrho}{\varrho}$ and $\varsigma = \left(\frac{2\gamma\Xi-2\Lambda-\sqrt{-2\Omega\gamma^2+4\Lambda^2}}{\gamma}\right)\frac{x^\rho}{\rho}+\gamma\frac{t^\varrho}{\varrho}$:

Solution class. M2.2.1 Hyperbolic function solutions (when $\Omega < 0$):

$$
\begin{aligned}
u_{\mathrm{M2,2,1}}(x,t) =& \mathrm{e}^{i\varsigma}\left(\frac{-\sqrt{-\frac{1}{\delta}}\left(\sqrt{-(g^2+h^2)\Omega}-g\sqrt{-\Omega}\cosh\left(2\sqrt{-\Omega}(\chi+\tau)\right)\right)}{\left(g\sinh\left(2\sqrt{-\Omega}(\chi+\tau)\right)+h\right)}\right),\\
v_{\mathrm{M2,2,1}}(x,t) =& -\frac{1}{2}\,\frac{\delta\gamma^2}{2\Lambda+\sqrt{-2\Omega\gamma^2+4\Lambda^2}}\left(\frac{-\sqrt{-\frac{1}{\delta}}\left(\sqrt{-(g^2+h^2)\Omega}-g\sqrt{-\Omega}\cosh\left(2\sqrt{-\Omega}(\chi+\tau)\right)\right)}{\left(g\sinh\left(2\sqrt{-\Omega}(\chi+\tau)\right)+h\right)}\right)^2+\Lambda,
\end{aligned}
\tag{5.32}
$$

$$
\begin{aligned}
u_{\mathrm{M2,2,2}}(x,t) =& \mathrm{e}^{i\varsigma}\left(-\sqrt{-\frac{1}{\delta}}\left(\sqrt{-\Omega}-\frac{2g\sqrt{-\Omega}}{g+\cosh\left(2\sqrt{-\Omega}(\chi+\tau)\right)-\sinh\left(2\sqrt{-\Omega}(\chi+\tau)\right)}\right)\right),\\
v_{\mathrm{M2,2,2}}(x,t) =& \frac{1}{2}\,\frac{\gamma^2}{2\Lambda+\sqrt{-2\Omega\gamma^2+4\Lambda^2}}\left(\left(\sqrt{-\Omega}-\frac{2g\sqrt{-\Omega}}{g+\cosh\left(2\sqrt{-\Omega}(\chi+\tau)\right)-\sinh\left(2\sqrt{-\Omega}(\chi+\tau)\right)}\right)\right)^2+\Lambda,
\end{aligned}
\tag{5.33}
$$

$$
\begin{aligned}
u_{\mathrm{M2,2,3}}(x,t) =& \mathrm{e}^{i\varsigma}\left(-\sqrt{-\frac{1}{\delta}}\sqrt{-\Omega}\tanh\left(\sqrt{-\Omega}(\chi+\tau)\right)\right),\\
v_{\mathrm{M2,2,3}}(x,t) =& -\frac{1}{2}\,\frac{\delta\gamma^2}{2\Lambda+\sqrt{-2\Omega\gamma^2+4\Lambda^2}}\left(-\sqrt{-\frac{1}{\delta}}\sqrt{-\Omega}\tanh\left(\sqrt{-\Omega}(\chi+\tau)\right)\right)^2+\Lambda,
\end{aligned}
\tag{5.34}
$$

and

$$\begin{aligned} u_{\mathrm{M2,2,4}}(x,t) =& \mathrm{e}^{i\varsigma}\Big(-\sqrt{-\frac{1}{\delta}}\,\sqrt{-\Omega}\coth\Big(\sqrt{-\Omega}\,(\chi+\tau)\Big)\Big), \\ v_{\mathrm{M2,2,4}}(x,t) =& -\frac{1}{2}\,\frac{\delta\,\gamma^2}{2\,\Lambda+\sqrt{-2\,\Omega\,\gamma^2+4\,\Lambda^2}}\Big(-\sqrt{-\frac{1}{\delta}}\,\sqrt{-\Omega}\coth\Big(\sqrt{-\Omega}\,(\chi+\tau)\Big)\Big)^2+\Lambda. \end{aligned} \tag{5.35}$$

Solution class. M2.2.2 Trigonometric function solutions (when $\Omega > 0$):

$$\begin{aligned} u_{\mathrm{M2,2,5}}(x,t) =& \mathrm{e}^{i\varsigma}\Big(\frac{-\sqrt{-\frac{1}{\delta}}\Big(\sqrt{(g^2-h^2)\,\Omega}-g\,\sqrt{\Omega}\cos\big(2\,\sqrt{\Omega}\,(\chi+\tau)\big)\Big)}{\big(g\sin\big(2\,\sqrt{\Omega}\,(\chi+\tau)\big)+h\big)}\Big), \\ v_{\mathrm{M2,2,5}}(x,t) =& -\frac{1}{2}\,\frac{\delta\,\gamma^2}{2\,\Lambda+\sqrt{-2\,\Omega\,\gamma^2+4\,\Lambda^2}}\Big(\frac{-\sqrt{-\frac{1}{\delta}}\Big(\sqrt{(g^2-h^2)\,\Omega}-g\,\sqrt{\Omega}\cos\big(2\,\sqrt{\Omega}\,(\chi+\tau)\big)\Big)}{\big(g\sin\big(2\,\sqrt{\Omega}\,(\chi+\tau)\big)+h\big)}\Big)^2+\Lambda, \end{aligned} \tag{5.36}$$

$$\begin{aligned} u_{\mathrm{M2,2,6}}(x,t) =& \mathrm{e}^{i\varsigma}\Big(-\sqrt{-\frac{1}{\delta}}\Big(i\,\sqrt{\Omega}-\frac{2\,ig\,\sqrt{\Omega}}{g+\cos\big(2\,\sqrt{\Omega}\,(\chi+\tau)\big)-\sin\big(2\,\sqrt{\Omega}\,(\chi+\tau)\big)}\Big)\Big), \\ v_{\mathrm{M2,2,6}}(x,t) =& \frac{1}{2}\,\frac{\gamma^2}{2\,\Lambda+\sqrt{-2\,\Omega\,\gamma^2+4\,\Lambda^2}}\Big(\Big(i\,\sqrt{\Omega}-\frac{2\,ig\,\sqrt{\Omega}}{g+\cos\big(2\,\sqrt{\Omega}\,(\chi+\tau)\big)-\sin\big(2\,\sqrt{\Omega}\,(\chi+\tau)\big)}\Big)\Big)^2+\Lambda, \end{aligned} \tag{5.37}$$

$$\begin{aligned} u_{\mathrm{M2,2,7}}(x,t) =& \mathrm{e}^{i\varsigma}\Big(-\sqrt{-\frac{\Omega}{\delta}}\tan\Big(\sqrt{\Omega}\,(\chi+\tau)\Big)\Big), \\ v_{\mathrm{M2,2,7}}(x,t) =& -\frac{1}{2}\,\frac{\delta\,\gamma^2}{2\,\Lambda+\sqrt{-2\,\Omega\,\gamma^2+4\,\Lambda^2}}\Big(-\sqrt{-\frac{\Omega}{\delta}}\tan\Big(\sqrt{\Omega}\,(\chi+\tau)\Big)\Big)^2+\Lambda, \end{aligned} \tag{5.38}$$

and

$$\begin{aligned} u_{\mathrm{M2,2,8}}(x,t) =& \mathrm{e}^{i\varsigma}\Big(\sqrt{-\frac{\Omega}{\delta}}\cot\Big(\sqrt{\Omega}\,(\chi+\tau)\Big)\Big), \\ v_{\mathrm{M2,2,8}}(x,t) =& -\frac{1}{2}\,\frac{\delta\,\gamma^2}{2\,\Lambda+\sqrt{-2\,\Omega\,\gamma^2+4\,\Lambda^2}}\Big(\sqrt{-\frac{\Omega}{\delta}}\cot\Big(\sqrt{\Omega}\,(\chi+\tau)\Big)\Big)^2+\Lambda. \end{aligned} \tag{5.39}$$

Solution class. M2.2.3 Rational function solutions (when $\Omega = 0$):

$$\begin{aligned} u_{\mathrm{M2,2,9}}(x,t) =& \mathrm{e}^{i\varsigma}\Big(\sqrt{-\frac{1}{\delta}}\,\frac{1}{(\chi+\tau)}\Big), \\ v_{\mathrm{M2,2,9}}(x,t) =& \frac{\gamma^2}{8\,\Lambda}\Big(\frac{1}{(\chi+\tau)}\Big)^2+\Lambda. \end{aligned} \tag{5.40}$$

6. Discussion

Numerous nonlinear soliton structures are produced by the system's interaction between dispersion, nonlinearity, and spin-field. In the scope of the model under study, we discovered that soliton structures can be either bright soliton, mix dark bright soliton, dark soliton, perturbed dark bright soliton, multi-soliton and periodic dark bright soliton. In the context of the FRSHMBS, a soliton is a self-reinforcing

solitary wave packet that maintains its speed and shape during propagation due to a precise balance between diffraction/dispersion and nonlinearity, mediated by coherent interaction with the medium's spin or polarization field. A dark soliton is a dip or notch in a continuous wave background, with a localized decrease in amplitude, which results from defocusing nonlinearity, possibly with damping or relaxation in the medium. Dark soliton indicates stable intensity depletion during propagation, seen in optical communication as phase slips or topological defects. A bright soliton on the other hand, is a localized pulse-like wave with intensity concentrated around a peak, surrounded by a zero or vanishing background that represents an optical pulse traveling without spreading due to coherent polarization support, which is important in optical fibers and ultrafast laser systems. In the context of FRSHMBS, this type of soliton may arise due to a dominant focusing nonlinearity, supported by gain from coherent spin-field interaction. A perturbed bright or dark soliton is a soliton with small fluctuations, ripples, or asymmetries in the shape, which may occur due to fractional effects, medium inhomogeneities, or relaxation terms. A bright-dark soliton is a mixed soliton where a bright soliton exists in one component and a dark soliton in another. This hybrid soliton shows intermodal energy exchange, which is crucial for signal switching and dual-mode communication that emerges due to cross-phase modulation between field and polarization, or coupling between components. A periodic bright-dark soliton is a periodically repeating structure combining dark and bright soliton forms that is related to soliton crystals or optical frequency combs in nonlinear optics. Finally, a multi-soliton is a solution involving one or more soliton structures. In our case, we have obtained a multi-soliton involving kink and dark or bright structure. Moreover, in our $2D$-plots, the core dynamics remains solitonic, but fractional effects introduce subtle variations. That is because, fractional-order derivatives introduce memory and nonlocal effects, which smooth or disturb the profile depending on the space-fractional order ρ. That is, when ρ is close to 1, the soliton profile remains almost the same with minimal perturbation. However, as ρ deviates from 1, then either amplitude changes or perturbation occurs. This indicates that effective dispersion or nonlinearity strength is modified and suggests that the soliton profile is less localized or shows pre-dispersion due to the system's memory.

In Figure 6, *A.* 3D and *B.* 2D visualize the dynamics of V-shaped dark soliton $u_{\mathrm{M1},1,3}(x,t)$, while *C.* 3D and *D.* 2D visualize the dynamics of a bell-shaped bright soliton $v_{\mathrm{M1},1,3}(x,t)$ explicitly presented in Eq (5.3). In Figure 7, *A.* 3D and *B.* 2D visualize the dynamics of a periodic V-shaped dark-bright soliton $u_{\mathrm{M1},1,4}(x,t)$, while *C.* 3D and *D.* 2D visualize the dynamics of a periodic U-shaped dark-bright soliton $v_{\mathrm{M1},1,4}(x,t)$ explicitly presented in Eq (5.4). In Figure 8, *A.* 3D and *B.* 2D visualize the dynamics of a bell-shaped bright soliton $u_{\mathrm{M1},2,1}(x,t)$, while *C.* 3D and *D.* 2D visualize the dynamics of a bell-shaped dark soliton $v_{\mathrm{M1},2,1}(x,t)$ explicitly presented in Eq (5.9). In Figure 9, *A.* 3D and *B.* 2D visualize the dynamics of a V-shaped dark soliton $u_{\mathrm{M1},2,7}(x,t)$, while *C.* 3D and *D.* 2D visualize the dynamics of a U-shaped parabolic dark soliton $v_{\mathrm{M1},2,7}(x,t)$ explicitly presented in Eq (5.15). In Figure 10, *A.* 3D and *B.* 2D visualize the dynamics of a bright kink-shaped multi-soliton $u_{\mathrm{M2},1,2}(x,t)$, while *C.* 3D and *D.* 2D visualize the dynamics of a dark kink-shaped multi-soliton $v_{\mathrm{M2},1,2}(x,t)$ explicitly presented in Eq (5.22). In Figure 11, *A.* 3D and *B.* 2D visualize the dynamics of a periodic V-shaped bright-dark soliton $u_{\mathrm{M2},1,5}(x,t)$, while *C.* 3D and *D.* 2D visualize the dynamics of a periodic U-shaped bright-dark soliton $v_{\mathrm{M2},1,5}(x,t)$ explicitly presented in Eq (5.25). In Figure 12, *A.* 3D and *B.* 2D visualize the dynamics of a perturbed V-shaped dark soliton $u_{\mathrm{M2},2,2}(x,t)$, while *C.* 3D and *D.* 2D visualize the dynamics of a perturbed U-shaped dark soliton $v_{\mathrm{M2},2,2}(x,t)$ explicitly presented in Eq (5.30). In Figure 13, *A.* 3D and *B.* 2D visualize the dynamics of a periodic bright soliton $u_{\mathrm{M2},2,6}(x,t)$, while *C.* 3D and *D.* 2D visualize

the dynamics of a periodic dark soliton $v_{M2,2,6}(x,t)$ explicitly presented in Eq (5.34).

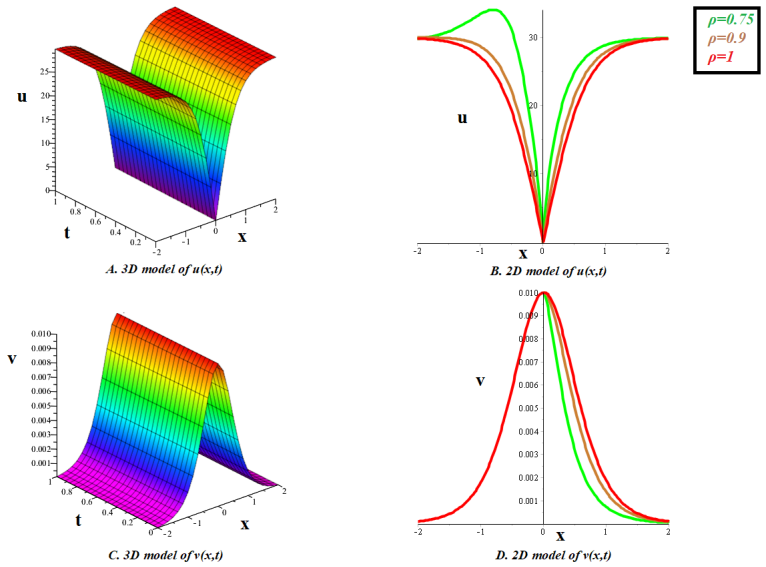

Figure 6. Soliton depictions of the dark soliton solution $u_{M1,1,3}(x,t)$ and bright soliton solution $v_{M1,1,3}(x,t)$ given in Eq (5.3) at $\Phi = 5, \Omega = 4, \Xi = 0.0010, \vartheta = 0.0030, \Lambda = 0.010, A_1 = 20, \rho = 1$, and $\varrho = 1$. Furthermore, the effect of the ρ-derivative on the solution for the given values is shown at $t = 1$.

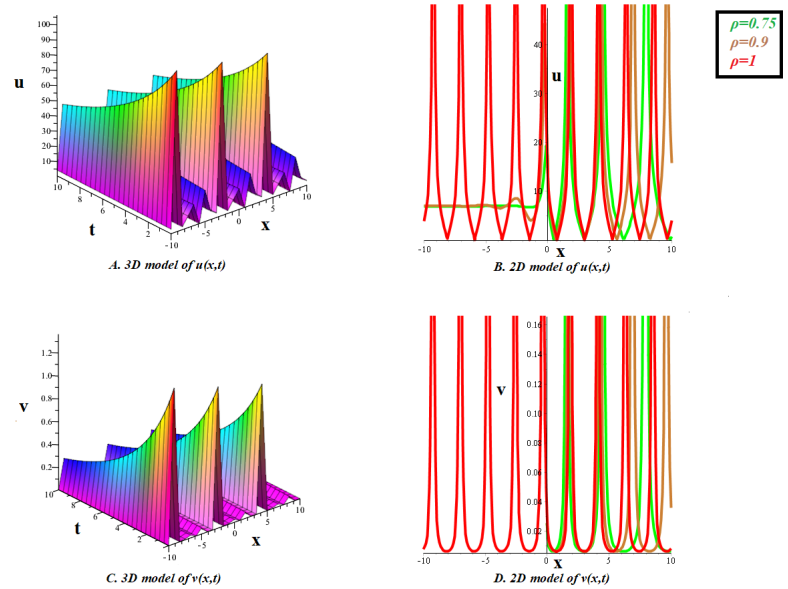

Figure 7. Soliton depictions of the bright soliton solutions $u_{M1,1,4}(x,t)$ and $v_{M1,1,4}(x,t)$ given in Eq (5.4) at $\Phi = 2, \Omega = 3, \Xi = 0.00550, \vartheta = 0.00450, \Lambda = 0.0060, A_1 = 5, \rho = 1, \varrho = 1, \xi_1 = 1$, and $\xi_2 = 2$. Furthermore, the effect of the ρ-derivative on the solution for the given values is shown at $t = 5$.

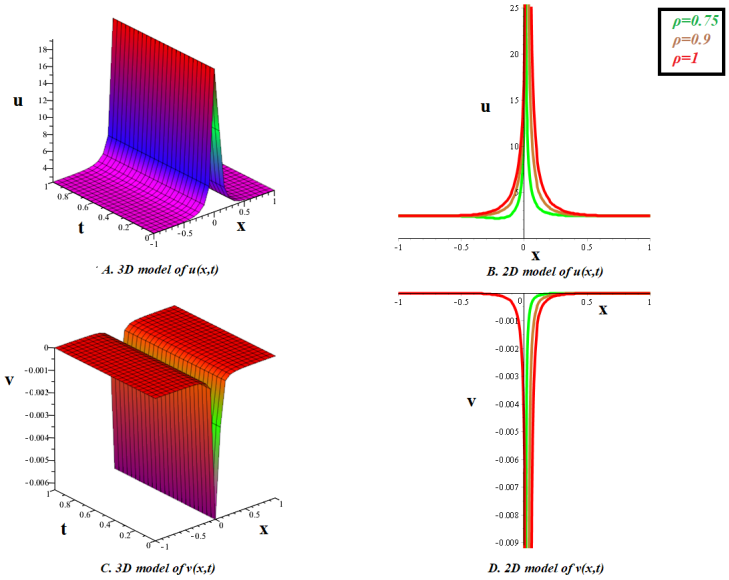

Figure 8. Soliton depictions of the bright soliton solution $u_{\mathrm{M1},2,1}(x,t)$ and dark soliton solution $v_{\mathrm{M1},2,1}(x,t)$ given in Eq (5.9) at $\Phi = 10, \Omega = 9, \Xi = 0.0075, \vartheta = 0.001150, \Lambda = 0.0001, A_0 = 3, \rho = 1, \varrho = 1, \xi_1 = 3$, and $\xi_2 = 4$. Furthermore, the effect of the ρ-derivative on the solution for the given values is shown at $t = 1$.

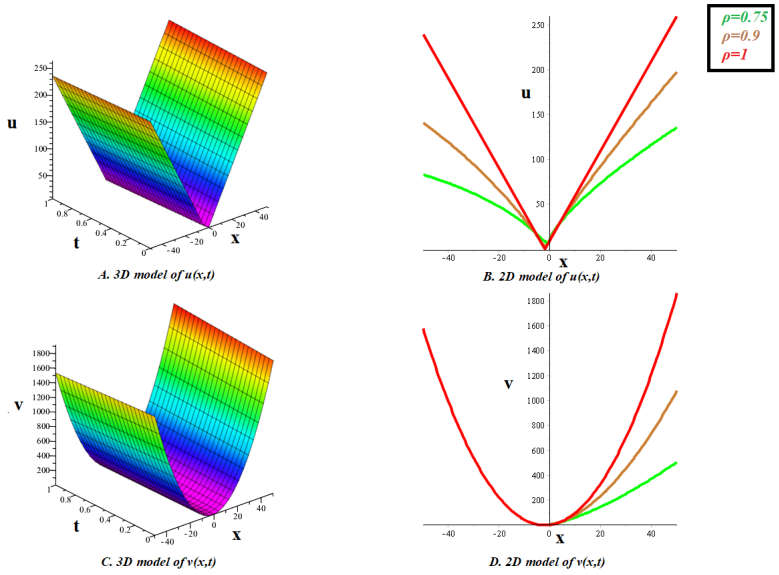

Figure 9. Soliton depictions of the dark soliton solutions $u_{\mathrm{M1},2,7}(x,t)$ and $v_{\mathrm{M1},2,7}(x,t)$ given in Eq (5.15) at $\Phi = 2, \Omega = 1, \Xi = 0.03, \vartheta = 0.02, \Lambda = 0.00055, A_0 = 5, \rho = 1, \varrho = 1, \xi_1 = 2$, and $\xi_2 = 5$. Furthermore, the effect of the ρ-derivative on the solution for the given values is shown at $t = 0.5$.

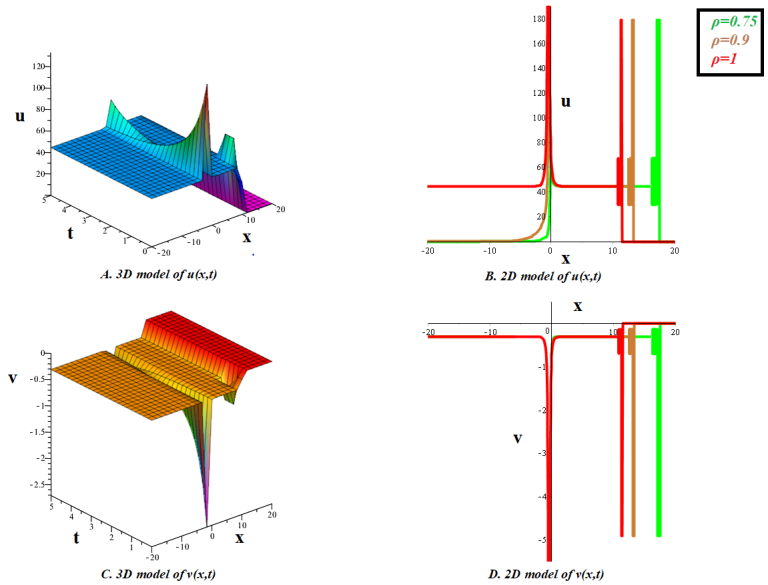

Figure 10. Soliton depictions of the kink-shaped multi-soliton solutions $u_{\mathrm{M2},1,2}(x,t)$ and $v_{\mathrm{M2},1,2}(x,t)$ given in Eq (5.22) at $\Omega = -3, \Xi = 0.0005, \delta = -0.0015, \Lambda = 0.00075, \gamma = 0.5, \rho = 1, \varrho = 1, g = 5$, and $\tau = 1$. Furthermore, the effect of the ρ-derivative on the solution for the given values is shown at $t = 5$.

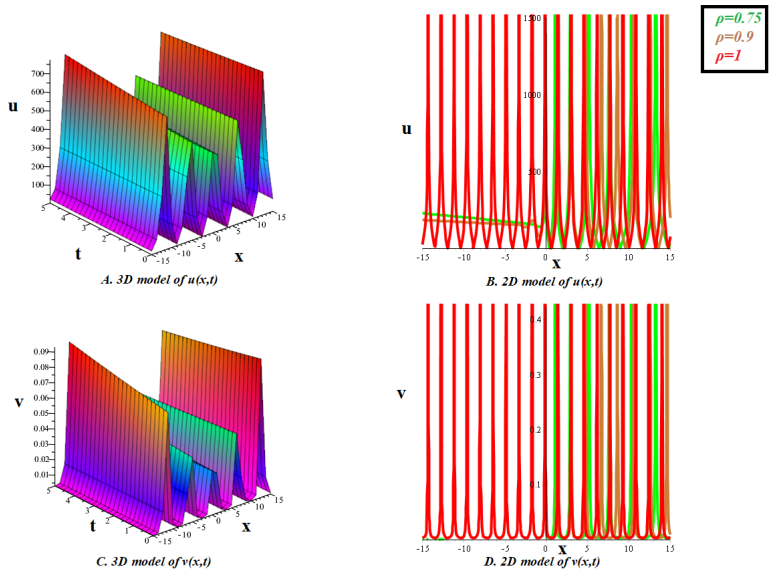

Figure 11. Soliton depictions of the bright soliton solutions $u_{\mathrm{M2},1,5}(x,t)$ and $v_{\mathrm{M2},1,5}(x,t)$ given in Eq (5.25) at $\Omega = 4, \Xi = 0.0001, \delta = 0.0002, \Lambda = 0.003, \gamma = 0.0001, \rho = 1, \varrho = 1, g = 2, h = 1$, and $\tau = 5$. Furthermore, the effect of the ρ-derivative on the solution for the given values is shown at $t = 5$.

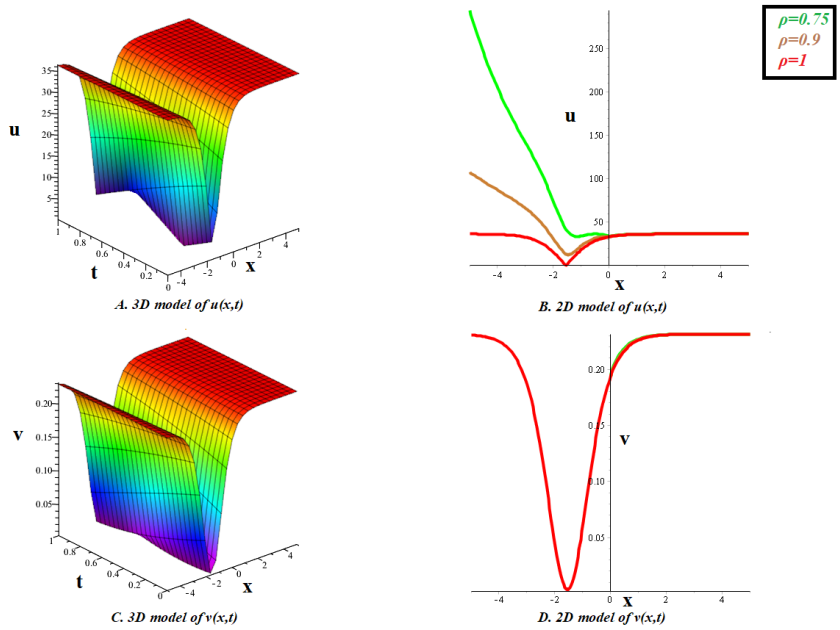

Figure 12. Soliton depictions of the dark soliton solutions $u_{\mathrm{M2,2,2}}(x,t)$ and $v_{\mathrm{M2,2,2}}(x,t)$ given in Eq (5.30) at $\Omega = -1, \Xi = 0.00025, \delta = -0.00075, \Lambda = 0.0035, \gamma = 0.65, \rho = 1, \varrho = 1, g = 3, h = 2$, and $\tau = 1$. Furthermore, the effect of the ρ-derivative on the solution for the given values is shown at $t = 0$.

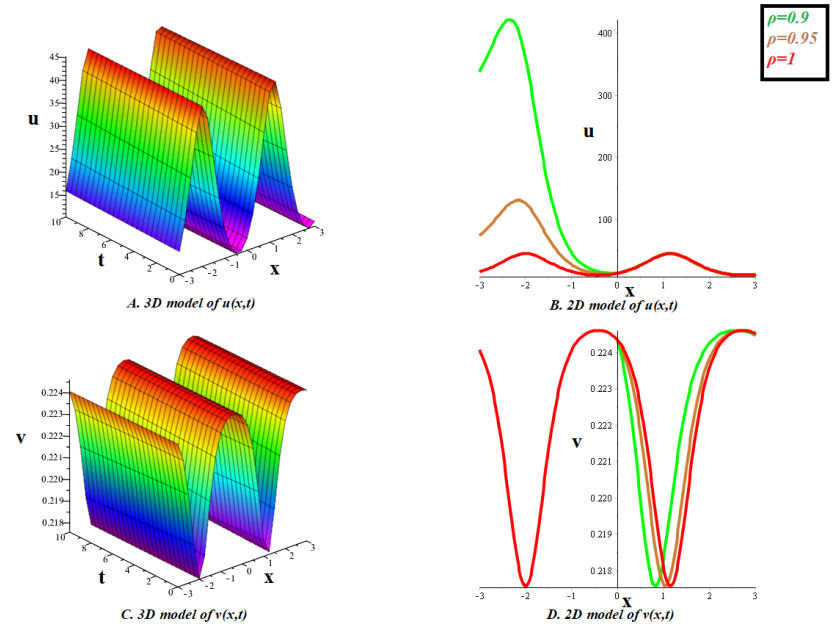

Figure 13. Soliton depictions of the periodic bright soliton solution $u_{\mathrm{M2,2,6}}(x,t)$ and periodic dark soliton solution $v_{\mathrm{M2,2,6}}(x,t)$ given in Eq (5.34) at $\Omega = 1, \Xi = 0.00555, \delta = -0.00215, \Lambda = 0.225, \gamma = 0.055, \rho = 1, \varrho = 1$, and $\tau = 0$. Furthermore, the effect of the ρ-derivative on the solution for the given values is shown at $t = 10$.

In addition to evaluating the soliton phenomena in the intended FRSHMBS, this work demonstrated the effectiveness of the (G'/G)-expansion approach and the suggested modified unified method in investigating the construction of soliton solutions for various models in nonlinear settings. The recommended methods, which provide closed form solutions, were selected because, like other approaches, they do not require intricate processes like linearization and perturbation. when dealing with nonlinear models. Because they provide many explicit solutions in five categories (rational, exponential, hyperbolic, trigonometric, and rational-hyperbolic functions), the suggested techniques are innovative and efficient. Because these solutions incorporate a broad class of wave formations that other methods would overlook or be unable to capture, they provide a more comprehensive understanding of the models' underlying process. It should be highlighted, nonetheless, that one of the approaches' shortcomings is that the homogeneous balancing principle fails to balance dispersion with the nonlinear term required to produce soliton solutions. Despite this drawback, this study demonstrates that the employed techniques are reliable and accurate for solving nonlinear problems in a range of scientific fields.

7. Conclusions

We investigated the integrable FRSHMBS with KFDs, an essential model for understanding the femtosecond pulses transmitted over an erbium-doped fiber. Analytical soliton solutions have been generated employing the (G'/G)-expansion approach and the modified unified method comprising the bright soliton, mix dark-bright soliton, dark soliton, perturbed dark and bright soliton, multi-soliton, and periodic dark-bright soliton. Some of the found solutions were dynamically shown using 2D and 3D graphs, illustrating the fundamental mechanics of the model. The impact of the space-fractional derivative on the given model was examined using the ρ-derivative framework, which provides a more dynamic and useful approach for bettering the accurateness of the results. In addition, under the Hamiltonian analysis, the planar system's phase portraits, and the perturbed system's time series plots were displayed using graphical representations to highlight the model's importance and dynamical behavior in the erbium-doped fiber. Our findings of this study are expected to have important ramifications for soliton theory, erbium-doped fiber, optical fibers, physical engineering, and nonlinear dynamics. Furthermore, we also proved that the modified unified approach and the $(\frac{G'}{G})$-expansion method are effective, robust, and simplistic strategies that produce a large number of soliton solutions that can be employed for NFPDEs in the mathematical sciences.

Future goal: Our future goal is to investigate the supplied model in the stochastic sense with some noise effects using novel approaches such as the Imetf method, Arnous method, and Kumar-Malik method and to conduct a thorough and exacting analysis of the discovered soliton solutions' stability.

Use of Generative-AI tools declaration

The author declares he has not used Artificial Intelligence (AI) tools in the creation of this article.

Acknowledgments

The author is thankful to the Deanship of Graduate Studies and Scientific Research at the University of Bisha for supporting this work through the Fast-Track Research Support Program.

Conflicts of interest

The author declares no conflict of interest in this paper.

Appendix

In this section, we present comparisons of the methods, list of abbreviations, and list of symbols.

A. Comparison of the methods

For the intended FRSHMBS, our suggested techniques produced a fresh multitude of optical soliton solutions. Limiting the solutions produced by (G'/G)-expansion technique results in the same solutions generated by modified unified method. This comparison is given in the following table:

Table A. Comparison of (G'/G)-expansion technique and modified unified method.

Family	**Solution's function**	**Solution**	(G'/G)-**expansion technique**	**Modified unified method**
Hyperbolic family	Coth function	$U(\chi) = \sqrt{\Pi}\coth(\frac{1}{2}\sqrt{\Pi}\chi)$	Given in Eq (5.5) for $A_1 = 2, \Pi > 0$	Given in Eq (5.26) for $\Omega = \frac{\Pi}{4}, \delta = -\frac{1}{4}, \Pi < 0$ and $\tau = 0$
	Tanh function	$U(\chi) = \sqrt{\Pi}\tanh(\frac{1}{2}\sqrt{\Pi}\chi)$	Given in Eq (5.6) for $A_1 = 2, \Pi > 0$	Given in Eq (5.27) for $\Omega = \frac{\Pi}{4}, \delta = -\frac{1}{4}, \Pi < 0$ and $\tau = 0$
Trigonometric family	Cot function	$U(\chi) = \sqrt{-\Pi}\cot(\frac{1}{2}\sqrt{-\Pi}\chi)$	Given in Eq (5.8) for $A_1 = 2, \Pi < 0$	Given in Eq (5.30) for $\Omega = -\frac{\Pi}{4}, \delta = -\frac{1}{4}, \Pi < 0$ and $\tau = 0$
	Tan function	$U(\chi) = -\sqrt{-\Pi}\tan(\frac{1}{2}\sqrt{-\Pi}\chi)$	Given in Eq (5.9) for $A_1 = 2, \Pi < 0$	Given in Eq (5.31) for $\Omega = -\frac{\Pi}{4}, \delta = -\frac{1}{4}, \Pi < 0$ and $\tau = 0$
Rational family	Rational function	$U(\chi) = \frac{1}{\chi}$	Given in Eq (5.11) for $A_1 = 1$	Given in Eq (5.40) for $\delta = -1$ and $\tau = 0$

B. List of abbreviations

NPDEs Nonlinear partial differential equations
NFPDEs Nonlinear fractional partial differential equations
RSHMBS Reduced spin Hirota-Maxwell-Bloch system

FRSHMBS	Fractional reduced spin Hirota-Maxwell-Bloch system
KFDs	Katugampola fractional derivatives
SIT	Self induced transparency

C. List of symbols

i	Imaginary unit
Ξ	Detuning from the erbium ion transitioning frequency
δ	Regulates the energy transfer between the medium and field
β, γ, ϑ	Wave numbers
Λ	Constant of integration

References

1. M. A. S. Murad, S. S. Mahmood, H. Emadifar, W. W. Mohammed, K. K. Ahmed, Optical soliton solution for dual-mode time-fractional nonlinear Schrödinger equation by generalized exponential rational function method, *Results Eng.*, **27** (2025), 105591. https://doi.org/10.1016/j.rineng.2025.105591
2. I. Alraddadi, F. Alsharif, S. Malik, H. Ahmad, T. Radwan, K. K. Ahmed, Innovative soliton solutions for a (2+1)-dimensional generalized KdV equation using two effective approaches, *AIMS Math.*, **9** (2024), 34966–34980. https://doi.org/10.3934/math.20241664
3. N. Alam, M. S. Ullah, J. Manafian, K. H. Mahmoud, A. S. A. Alsubaie, H. M. Ahmed, et al., Bifurcation analysis, chaotic behaviors, and explicit solutions for a fractional two-mode Nizhnik-Novikov-Veselov equation in mathematical physics, *AIMS Math.*, **10** (2025), 4558–4578. https://doi.org/10.3934/math.2025211
4. I. Samir, H. M. Ahmed, H. Emadifar, K. K. Ahmed, Traveling and soliton waves and their characteristics in the extended (3+1)-dimensional Kadomtsev-Petviashvili equation in fluid, *Partial Differ. Equ. Appl. Math.*, **14** (2025), 101146. https://doi.org/10.1016/j.padiff.2025.101146
5. A. Khalifa, H. Ahmed, K. K. Ahmed, Construction of exact solutions for a higher-order stochastic modified Gerdjikov-Ivanov model using the Imetf method, *Phys. Scr.*, 2024. https://doi.org/10.1088/1402-4896/ada321
6. J. R. M. Borhan, E. I. Hassan, A. Dawood, K. Aldwoah, A. I. A. Sayed, A. Albaity, et al., Chaotic behaviour, sensitivity assessment, and new analytical investigation to find novel optical soliton solutions of M-fractional Kuralay-II equation, *Mathematics*, **13** (2025), 2207. https://doi.org/10.3390/math13132207
7. U. N. Katugampola, A new fractional derivative with classical properties, *arXiv Preprint*, 2014. https://doi.org/10.48550/arXiv.1410.6535
8. C. Qiao, X. Long, L. Yang, Y. Zhu, W. Cai, Calculation of a dynamical substitute for the real Earth-Moon system based on Hamiltonian analysis, *Astrophys. J.*, **991** (2025), 46. https://doi.org/10.3847/1538-4357/adf73a
9. Z. Chong, C. Wang, H. Zhang, S. Zhang, Sine-transform-based dual-memristor hyperchaotic map and analog circuit implementation, *IEEE Trans. Instrum. Meas.*, **74** (2025), 1–14. https://doi.org/10.1109/TIM.2025.3570347

10. W. Sun, Y. Jin, G. Lu, Y. Liu, Stabilizer testing and central limit theorem, *Phys. Rev. A*, **111** (2025), 032421. https://doi.org/10.1103/PhysRevA.111.032421

11. X. Guo, J. Zhang, X. Meng, Z. Li, X. Wen, P. Girard, et al., HALTRAV: design of a high-performance and area-efficient latch with triple-node-upset recovery and algorithm-based verifications, *IEEE Trans. Comput.-Aided Des. Integr. Circuits Syst.*, **44** (2025), 2367–2377. https://doi.org/10.1109/TCAD.2024.3511335

12. R. Ali, Z. Zhang, H. Ahmad, Exploring soliton solutions in nonlinear spatiotemporal fractional quantum mechanics equations: an analytical study, *Opt. Quant. Electron.*, **56** (2024), 838. https://doi.org/10.1007/s11082-024-06370-2

13. G. Akram, M. Sadaf, S. Arshed, R. Latif, M. Inc, A. S. M. Alzaidi, Exact traveling wave solutions of (2+1)-dimensional extended Calogero-Bogoyavlenskii-Schiff equation using extended trial equation method and modified auxiliary equation method, *Opt. Quant. Electron.*, **56** (2024), 424. https://doi.org/10.1007/s11082-023-05900-8

14. K. Suwais, N. Mlaiki, S. Barak, R. Ali, Novel quasi-periodic type optical solitons and the formation of fractal structures in non-integrable nonlinear Helmholtz equations with phase portraits and chaotic analysis, *Eur. J. Pure Appl. Math.*, **18** (2025), 6764–6764. https://doi.org/10.29020/nybg.ejpam.v18i4.6764

15. I. Samir, H. M. Ahmed, W. Rabie, W. Abbas, O. Mostafa, Construction optical solitons of generalized nonlinear Schrödinger equation with quintuple power-law nonlinearity using Exp-function, projective Riccati, and new generalized methods, *AIMS Math.*, **10** (2025), 3392–3407. https://doi.org/10.3934/math.2025157

16. A. Farooq, M. I. Khan, W. X. Ma, Exact solutions for the improved mKdv equation with conformable derivative by using the Jacobi elliptic function expansion method, *Opt. Quant. Electron.*, **56** (2024), 542. https://doi.org/10.1007/s11082-023-06258-7

17. K. A. Gepreel, T. A. Nofal, A. A. Alasmari, Exact solutions for nonlinear integro-partial differential equations using the generalized Kudryashov method, *J. Egypt. Math. Soc.*, **25** (2017), 438–444. https://doi.org/10.1016/j.joems.2017.09.001

18. N. M. Tuan, N. H. Son, Hirota bilinear performance on Hirota-Satsuma-Ito equation using bilinear neural network method, *Int. J. Appl. Comput. Math.*, **11** (2025), 121. https://doi.org/10.1007/s40819-025-01933-7

19. Z. Aydın, F. Tascan, Application of new Kudryashov method to Sawada-Kotera and Kaup-Kupershmidt equations, *Comput. Methods Differ. Equ.*, **13** (2025), 608–617. https://doi.org/10.22034/cmde.2024.60001.2558

20. S. Behera, Analysis of traveling wave solutions of two space-time nonlinear fractional differential equations by the first-integral method, *Mod. Phys. Lett. B*, **38** (2024), 2350247. https://doi.org/10.1142/S0217984923502470

21. A. M. Wazwaz, The sine-cosine method for obtaining solutions with compact and noncompact structures, *Appl. Math. Comput.*, **159** (2004), 559–576. https://doi.org/10.1016/j.amc.2003.08.136

22. E. M. E. Zayed, A. G. Al-Nowehy, The modified simple equation method, the exp-function method, and the method of soliton ansatz for solving the long-short wave resonance equations, *Z. Naturforsch. A*, **71** (2016), 103–112. https://doi.org/10.1515/zna-2015-0414

23. E. J. Parkes, Observations on the tanh-coth expansion method for finding solutions to nonlinear evolution equations, *Appl. Math. Comput.*, **217** (2010), 1749–1754. https://doi.org/10.1016/j.amc.2009.11.037

24. A. R. Alharbi, M. B. Almatrafi, New exact and numerical solutions with their stability for Ito integro-differential equation via Riccati–Bernoulli sub-ODE method, *J. Taibah Univ. Sci.*, **14** (2020), 1447–1456. https://doi.org/10.1080/16583655.2020.1827853

25. S. Noor, A. S. Alshehry, A. Shafee, R. Shah, Families of propagating soliton solutions for (3+1)-fractional Wazwaz-BenjaminBona-Mahony equation through a novel modification of modified extended direct algebraic method, *Phys. Scr.*, **99** (2024), 045230. https://doi.org/10.1088/1402-4896/ad23b0

26. M. B. Almatrafi, Solitary wave solutions to a fractional-order Fokas equation via the improved modified extended tanh-function approach, *Mathematics*, **13** (2025), 109. https://doi.org/10.3390/math13010109

27. R. Ali, S. Barak, A. Altalbe, Analytical study of soliton dynamics in the realm of fractional extended shallow water wave equations, *Phys. Scr.*, **99** (2024), 065235. https://doi.org/10.1088/1402-4896/ad4784

28. H. Khan, S. Barak, P. Kumam, M. Arif, Analytical solutions of fractional Klein-Gordon and gas dynamics equations, via the (G'/G)-expansion method, *Symmetry*, **11** (2019), 566. https://doi.org/10.3390/sym11040566

29. N. Raza, M. H. Rafiq, M. Kaplan, S. Kumar, Y. M. Chu, The unified method for abundant soliton solutions of local time fractional nonlinear evolution equations, *Results Phys.*, **22** (2021), 103979. https://doi.org/10.1016/j.rinp.2021.103979

30. A. J. A. M. Jawad, M. D. Petkovic, A. Biswas, Modified simple equation method for nonlinear evolution equations, *Appl. Math. Comput.*, **217** (2010), 869–877. https://doi.org/10.1016/j.amc.2010.06.030

31. S. A. El-Tantawy, H. A. Alyousef, R. T. Matoog, R. Shah, On the optical soliton solutions to the fractional complex structured (1+1)-dimensional perturbed Gerdjikov-Ivanov equation, *Phys. Scr.*, **99** (2024), 035249. https://doi.org/10.1088/1402-4896/ad241b

32. H. Yasmin, A. W. Alrowaily, M. Areshi, R. Shah, S. A. El-Tantawy, On the analytical soliton-like solutions to (2+1)-dimensional fractional asymmetric Nizhnik-Novikov-Veselov system arising in incompressible fluids, *Front. Phys.*, **12** (2024), 1443986. https://doi.org/10.3389/fphy.2024.1443986

33. N. Iqbal, W. W. Mohammed, A. E. Hamza, S. Hussain, Y. Jawarneh, R. Shah, Fractals and chaotic solitons phenomena in conformable coupled Higgs system, *Discrete Dyn. Nat. Soc.*, **2025** (2025), 1–16. https://doi.org/10.1155/ddns/8384630

34. Z. Li, Optical solutions of the nonlinear Kodama equation with the M-truncated derivative via the extended (G'/G)-expansion method, *Fractal Fract.*, **9** (2025), 300. https://doi.org/10.3390/fractalfract9050300

35. S. Behera, Optical solitons for the Hirota-Ramani equation via improved $(\frac{G'}{G})$-expansion method, *Mod. Phys. Lett. B*, **39** (2025), 2450403. https://doi.org/10.1142/S0217984924504037

36. T. Aydemir, Comparative analysis of the generalized unified method with some exact solution methods and general solutions of the Biswas-Milovic equation, *Theor. Math. Phys.*, **222** (2025), 119–130. https://doi.org/10.1134/S004057792501009X

37. N. Raza, M. H. Rafiq, M. Kaplan, S. Kumar, Y. M. Chu, The unified method for abundant soliton solutions of local time fractional nonlinear evolution equations, *Results Phys.*, **22** (2021), 103979. https://doi.org/10.1016/j.rinp.2021.103979

38. X. H. Wu, Y. T. Gao, X. Yu, L. Q. Li, C. C. Ding, Vector breathers, rogue and breather-rogue waves for a coupled mixed derivative nonlinear Schrödinger system in an optical fiber, *Nonlinear Dyn.*, **111** (2023), 5641–5653. https://doi.org/10.1007/s11071-022-08058-2

39. L. Salmela, N. Tsipinakis, A. Foi, C. Billet, J. M. Dudley, G. Genty, Predicting ultrafast nonlinear dynamics in fibre optics with a recurrent neural network. *Nat. Mach. Intell.*, **3** (2021), 344–354. https://doi.org/10.1038/s42256-021-00297-z

40. J. Zhao, J. Dai, B. Braverman, X. C. Zhang, R. W. Boyd, Compressive ultrafast pulse measurement via time-domain single-pixel imaging, *Optica*, **8** (2021), 1176–1185. https://doi.org/10.1364/OPTICA.431455

41. X. H. Wu, Y. T. Gao, Generalized Darboux transformation and solitons for the Ablowitz-Ladik equation in an electrical lattice, *Appl. Math. Lett.*, **137** (2023), 108476. https://doi.org/10.1016/j.aml.2022.108476

42. S. A. El-Tantawy, A. H. Salas, H. A. Alyousef, M. R. Alharthi, Novel approximations to a nonplanar nonlinear Schrödinger equation and modeling nonplanar rogue waves/breathers in a complex plasma, *Chaos, Soliton. Fract.*, **163** (2022), 112612. https://doi.org/10.1016/j.chaos.2022.112612

43. M. Tlidi, M. Taki, Rogue waves in nonlinear optics, *Adv. Opt. Photonics*, **14** (2022), 87–147. https://doi.org/10.1364/AOP.438025

44. J. Guo, X. Hu, J. Ma, L. Zhao, D. Shen, D. Tang, Anti-dark solitons in a single mode fiber laser, *Phys. Lett. A*, **395** (2021), 127226. https://doi.org/10.1016/j.physleta.2021.127226

45. S. K. Hazra, P. K. Pathak, T. N. Dey, Self-induced transparency in a semiconductor quantum dot medium at ultracold temperatures, *Phys. Rev. B*, **107** (2023), 235409. https://doi.org/10.1103/PhysRevB.107.235409

46. A. Pakhomov, M. Arkhipov, N. Rosanov, R. Arkhipov, Self-starting coherent mode locking in a two-section laser with identical gain and absorber media, *Phys. Rev. A*, **107** (2023), 013510. https://doi.org/10.1103/PhysRevA.107.013510

47. X. Q. Cui, B. J. Zhang, X. Y. Wen, Bright-dark soliton solutions and their elastic interaction analysis for a reduced integrable spin Hirota-Maxwell-Bloch equation, *Chinese J. Phys.*, **82** (2023), 95–104. https://doi.org/10.1016/j.cjph.2023.01.006

48. B. Ceesay, M. W. Yasin, N. Ahmed, M. Z. Baber, E. Bittaye, Revealing homoclinic breather waves, periodic lump waves and other waves forms of an integrable reduced spin Hirota-Maxwell-Bloch system, *Sci. Rep.*, **15** (2025), 1–17. https://doi.org/10.1038/s41598-025-95093-9

49. G. H. Tipu, K. Anwar, F. Yao, U. Younas, Analytical exploration of optical structures in an integrable reduced spin Hirota-Maxwell-Bloch system, 2025. https://doi.org/10.21203/rs.3.rs-6778005/v1

50. J. Wang, Z. Li, The impact of standard Wiener process on the qualitative analysis and traveling wave solutions of stochastic nonlinear Kodama equation in the Stratonovich sense, *AIMS Math.*, **10** (2025), 24997–25010. https://doi.org/10.3934/math.20251107

51. Z. Li, Traveling wave solutions, numerical simulation and phase portraits for the conformable space-time fractional diffusive predator-prey system, *Phys. Lett. A*, **561** (2025), 130995. https://doi.org/10.1016/j.physleta.2025.130995

AIMS Press